



THE STATE OF THE CLIMATE 2022

Ole Humlum

The State of the Climate 2022

Ole Humlum

Report 56, The Global Warming Policy Foundation

© Copyright 2023, The Global Warming Policy Foundation

About the author

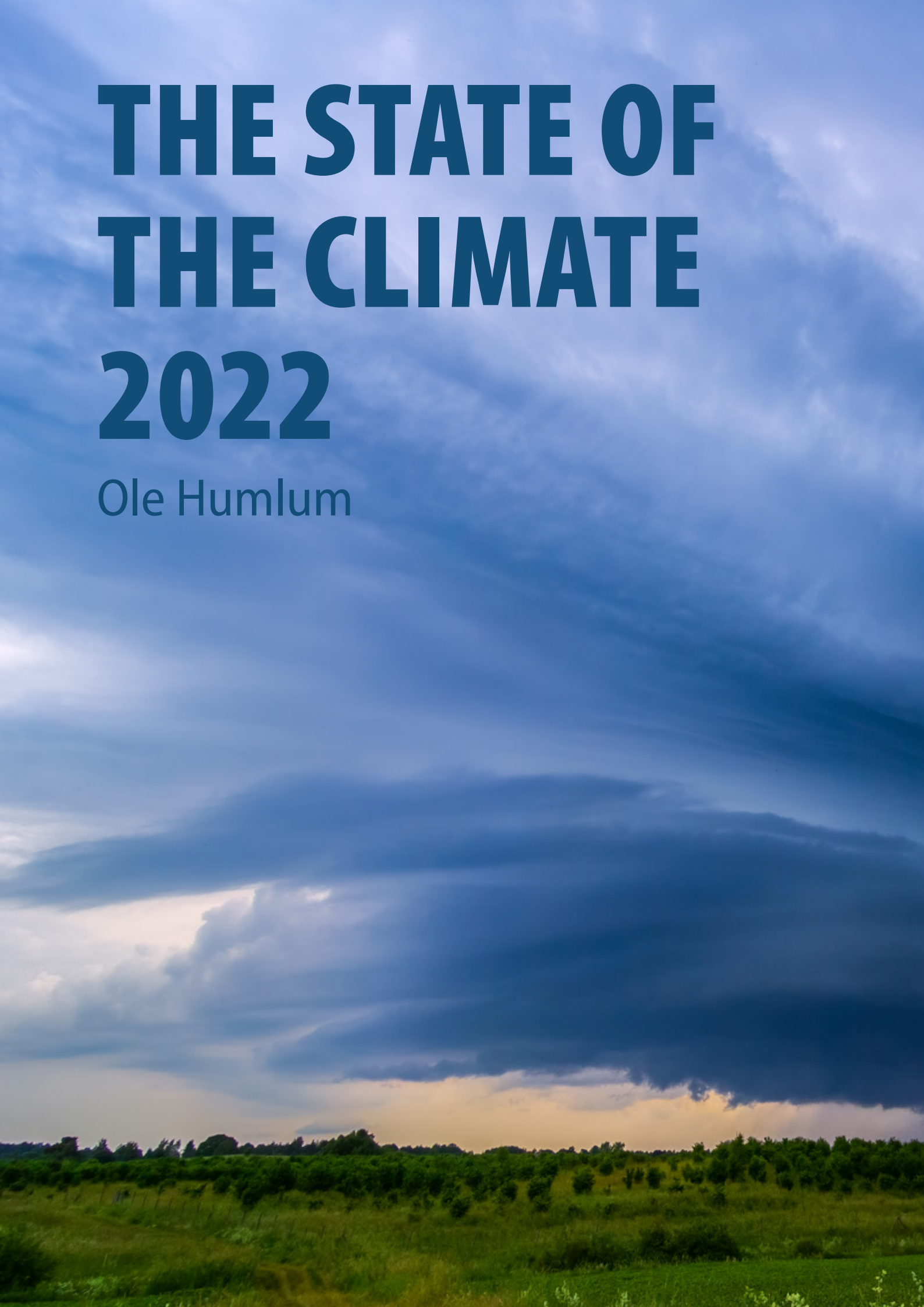
Ole Humlum is former Professor of Physical Geography at the University Centre in Svalbard, Norway, and Emeritus Professor of Physical Geography, University of Oslo, Norway.



Contents

<i>About the author</i>	ii
<i>General summary</i>	2
1. Air temperatures	4
2. Atmospheric greenhouse gases	19
3. Ocean temperatures	22
4. Oceanic oscillations	31
5. Sea-level	33
6. Snow and ice	38
7. Tropical storm and hurricanes	42
<i>Written references</i>	46
<i>Data sources</i>	46
<i>Review process</i>	48
<i>About the Global Warming Policy Foundation</i>	48





THE STATE OF THE CLIMATE 2022

Ole Humlum



General summary

This report has its focus on observations, and not on output from numerical models, with a few exceptions (e.g. Figure 38). References and data sources are listed at the end of the report.

Air temperatures

Average air temperatures measured near the planet's surface (surface air temperatures), or rather their deviation from the average calculated for a chosen reference period, are central to many climate deliberations. However, the significance of any short-term warming or cooling recorded in these datasets should not be overstated. Firstly, focusing on averages tends to hide the fact that we all deal with much larger temperature variations on a daily basis. Secondly, whenever Earth experiences warm El Niño or cold La Niña episodes, major heat exchanges take place between the Pacific Ocean and the atmosphere above, eventually showing up as a signal in the global air temperature. However, these do not reflect similar changes in the total heat content of the atmosphere-ocean system. In fact, the global net changes involved may be small; such heat exchanges may chiefly reflect redistribution of energy between ocean and atmosphere. Evaluating the dynamics of ocean temperatures is therefore equally as important as evaluating changes in surface air temperatures.

Relative to the whole period since 1850/1880, 2022 was warm, but cooler than most years since 2016. A moderate La Niña episode played out during the year, underlining the importance of ocean-atmosphere exchanges.

Many Arctic regions experienced record high air temperatures in 2016, but since then, including in 2022, conditions generally have turned somewhat cooler. The Arctic temperature peak in 2016 may have been affected by ocean heat, released from the Pacific Ocean during the strong 2015–16 El Niño and subsequently transported towards the Arctic. This underscores how Arctic air temperatures may be affected, not only by variations in local conditions, but also by variations playing out in geographically remote regions.

Many diagrams in this report focus on the

time from 1979 onwards, reflecting the start of the satellite era, and the advent of a wide range of observations with nearly global coverage, including temperature. These data give a detailed view of temperature changes over time at different altitudes in the atmosphere. Among other phenomena, they reveal that a Stratospheric temperature plateau has prevailed since 1995.

Since 1979, temperatures in the lower Troposphere have increased over both land and oceans, but most clearly over land. The most straightforward explanation for this observation is that much of the warming is caused by solar insolation, but there may well be several supplementary reasons, such as differences in heat capacity and changes in cloud cover and land use.

Oceans

The Argo program has now achieved 19 years of global coverage, growing from a relatively sparse array of 1000 profiling floats in 2004, to more than 3900 in December 2021. Since their inception, these have provided a unique ocean temperature dataset for depths down to 1900 m. The data is currently updated to August 2020. Although the oceans are much deeper than 1900 m, and the dataset is still relatively short, interesting features are now emerging from these observations.

Globally, since 2004, the upper 1900 m of the oceans have experienced net warming of about 0.07°C. The maximum net warming (about 0.2°C) affects the uppermost 100 m. This is seen mainly in regions near the Equator, where the greatest amount of solar radiation is received. At greater depths, a small (about 0.025°C) net warming has occurred between 2004 and 2020.

This development in global average ocean temperatures is reflected across the Equatorial oceans, between 30°N and 30°S, which, because of the spherical form of the planet, represent a huge surface area. However, simultaneously, the northern oceans (55–65°N) have on average experienced a marked cooling down to 1400 m depth, and slight warming below that. The southern oceans (55–65°S) have on average seen slight warming at most depths since 2004,

but mainly near the surface. However, averages may be misleading, and quite often better insight is obtained by studying the details, as discussed later in this report.

Sea level

Sea level is monitored by satellite altimetry and by direct measurements using tide gauges situated along coasts. While the satellite-derived record suggests a global sea level rise of about 3.4 mm per year or more, data from tide gauges all over the world suggest a stable average global sea-level rise of 1–2 mm per year. The measurements do not indicate any recent acceleration (or deceleration). The marked difference (a ratio of about 1:2) between the two datasets still has no universally accepted explanation, but it is known that satellite observations of sea level are complicated in areas near the coast (see, e.g., Vignudelli et al. 2019). Either way, for local coastal planning, the tide-gauge data is preferred, as explained later in this report.

Sea ice

In 2022, global sea-ice cover remained well below the average for the satellite era (since 1979), but now with a stable or even rising global trend indicated. At the end of 2016, global sea-ice extent reached a marked minimum, at least partly caused by the operation of two different natural cycles characterising sea ice in the Northern- and Southern Hemispheres, respectively. The two cycles had simultaneous minima in 2016, with consequences for the global sea-ice extent. The opposite development, towards stable or higher sea-ice extent at both poles, probably began in 2018, and has since become more pronounced. The marked Antarctic sea ice

reduction in 2016 was also affected by unusual wind conditions.

Snow cover

Variations in global snow cover are mainly caused by changes in the Northern Hemisphere, where all the major land areas are located. The Southern Hemisphere snow cover extent is essentially controlled by the Antarctic Ice Sheet, and therefore relatively stable. The Northern Hemisphere average snow cover extent has also been more or less static since the onset of satellite observations, although local and regional interannual variations may be large. Considering seasonal changes in the Northern Hemisphere since 1979, autumn extent is slightly increasing, mid-winter extent is basically stable, and spring extent is slightly decreasing. In 2022, the Northern Hemisphere seasonal snow cover extent was near the 1972–2021 average.

Storms and hurricanes

The most recent data on global tropical storm and hurricane accumulated cyclone energy (ACE) is well within the range seen since 1970. The ACE series displays a variable pattern over time, with a significant 3.6-year variation, but without any clear trend towards higher or lower values. A longer ACE series for the Atlantic Basin (since 1850), however, suggests natural rhythms of 55.8- and 7.8-years' duration. In addition, modern data on the number of hurricane land-falls in the continental United States remains within the normal range throughout the entire observation period since 1851.

1. Air temperatures

Surface: spatial pattern

Global average surface air temperature for 2022 was nearly identical to the previous year, and it increasingly looks as if 2016 may indicate a global temperature peak (Figure 1). The coming years will show if this is correct or not. 2022 was – like 2021 – affected by a cold La Niña episode (Pacific Ocean, see Figure 29).

The Northern Hemisphere was characterised by regional temperature contrasts, especially above 30°N. The most pronounced temperature events in 2022 were low average temperatures in much of North America and the oceans around Greenland and northern Europe. In contrast, much of Europe and the Russia-Siberia regions had relatively high temperatures in 2022 (compared to the last 10 years).

In the Arctic, the Europe-Russia-Siberia sectors were relatively warm, while much of the Canada-Alaska sector was relatively cool (Figure 2a).

Near the Equator, surface air temperatures were generally near or below the average for the previous 10 years. In the Pacific Ocean, cool conditions reflected the ongoing La Niña episode.

In the Southern Hemisphere, surface air temperatures were near or below the average for the previous 10 years. All major land areas were cool in 2022 compared to the previous 10 years.

The oceans around the Antarctic continent were relatively warm in 2022, as was most of West Antarctica. East Antarctica was near or below the 10-year average (Figure 2b).

Summing up for 2022, global average air temperatures were high relative to a long instrumental record (since 1850), but with suggestions of an overall negative trend since 2016. However, they were influenced by an ongoing La Niña episode in the Pacific Ocean.

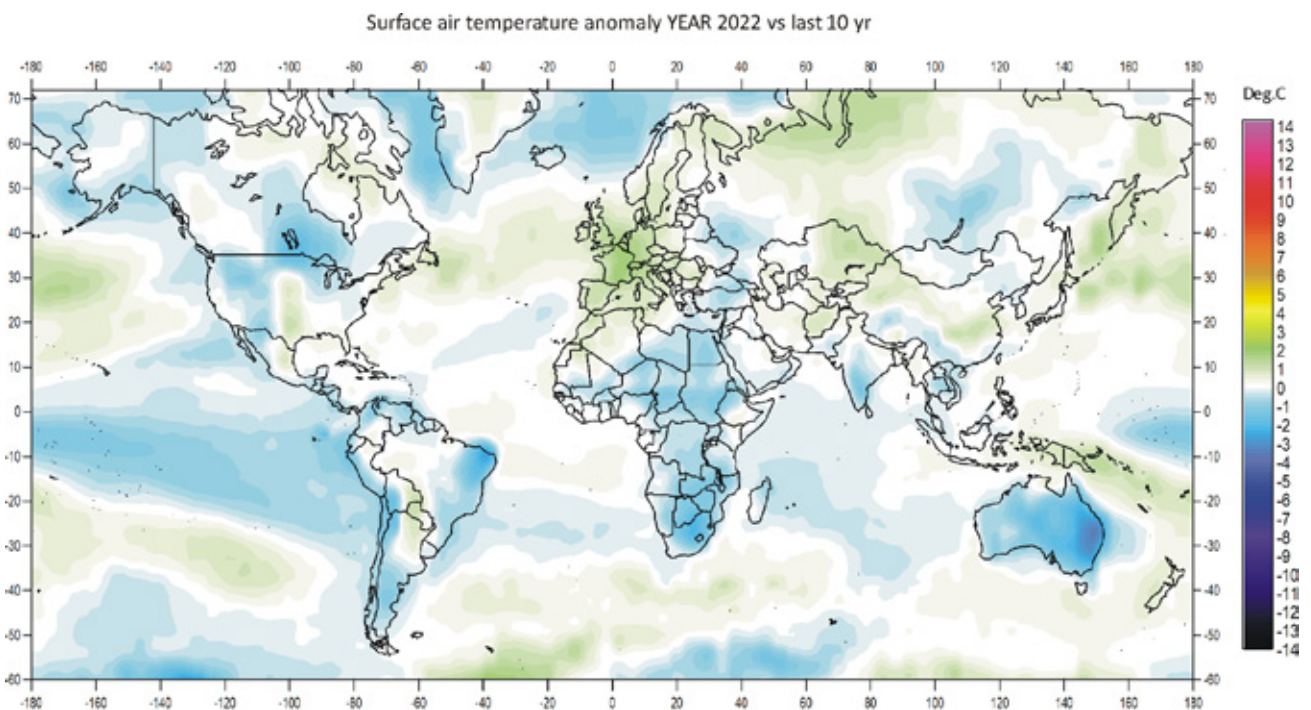


Figure 1: 2022 surface air temperatures compared to the average for the previous 10 years.

Green-yellow-red colours indicate areas with higher temperature than the average, while blue colours indicate lower than average temperatures. Data source: Remote Sensed Surface Temperature Anomaly, AIRS/Aqua L3 Monthly Standard Physical Retrieval 1-degree x 1-degree V007 (<https://airs.jpl.nasa.gov/>), obtained from the GISS data portal (https://data.giss.nasa.gov/gistemp/maps/index_v4.html).

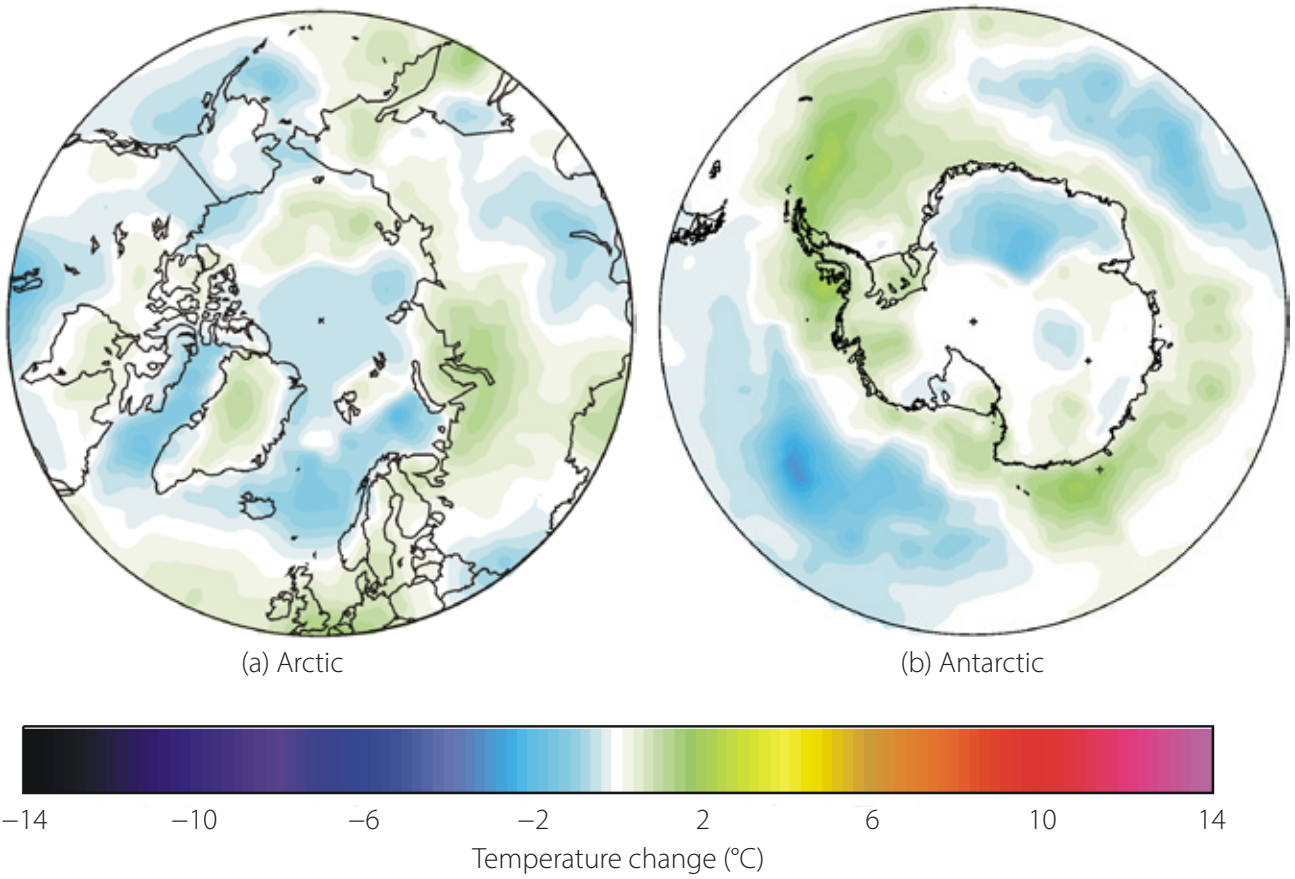
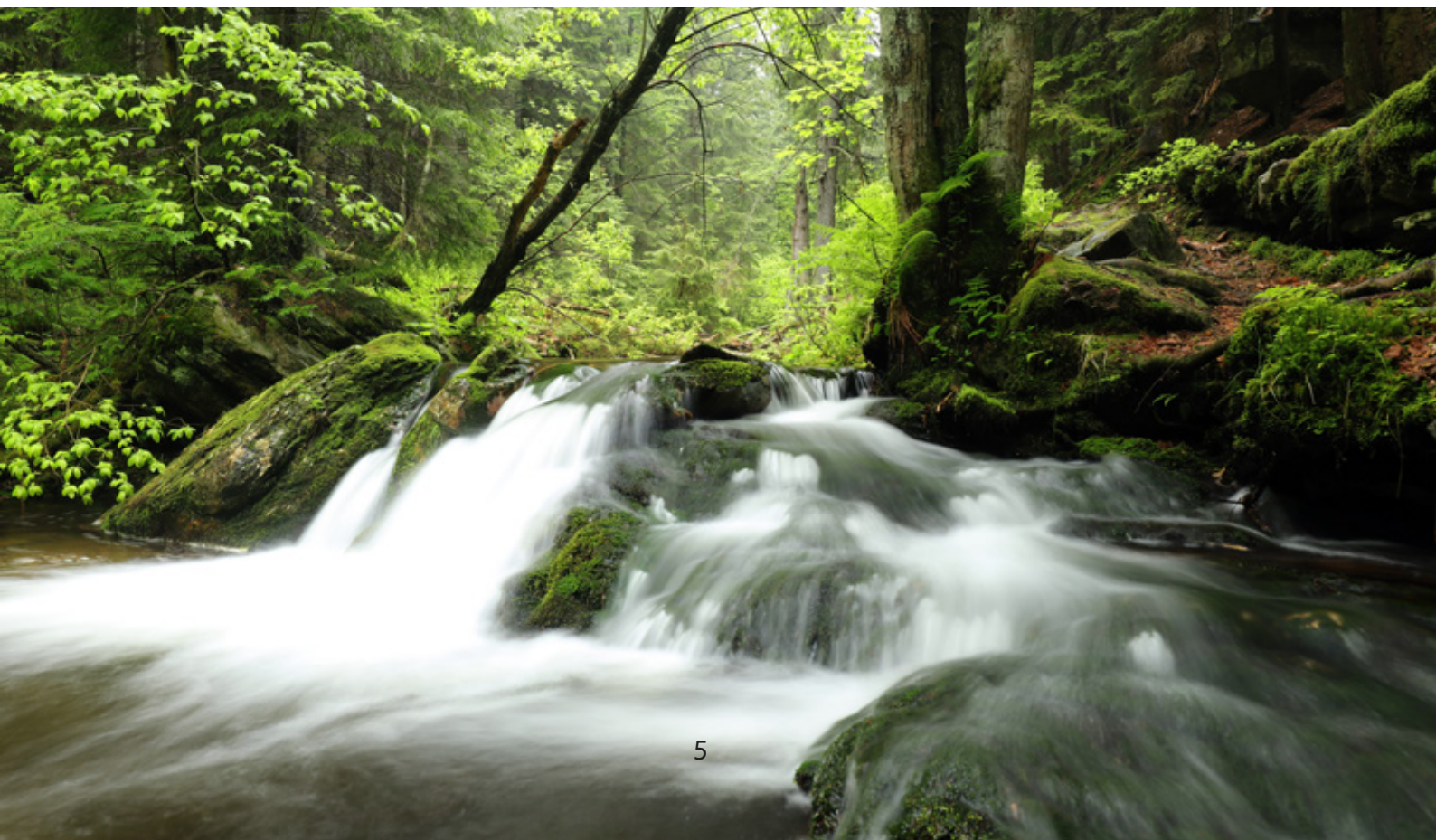


Figure 2: 2022 polar surface air temperatures compared to the average for the previous 10 years.

Green-yellow-red colours indicate areas with higher temperature than the average, while blue colours indicate lower than average temperatures. Data source: Remote Sensed Surface Temperature Anomaly, AIRS/Aqua L3 Monthly Standard Physical Retrieval 1-degree x 1-degree V007 (<https://airs.jpl.nasa.gov/>), obtained from the GISS data portal (https://data.giss.nasa.gov/gistemp/maps/index_v4.html).

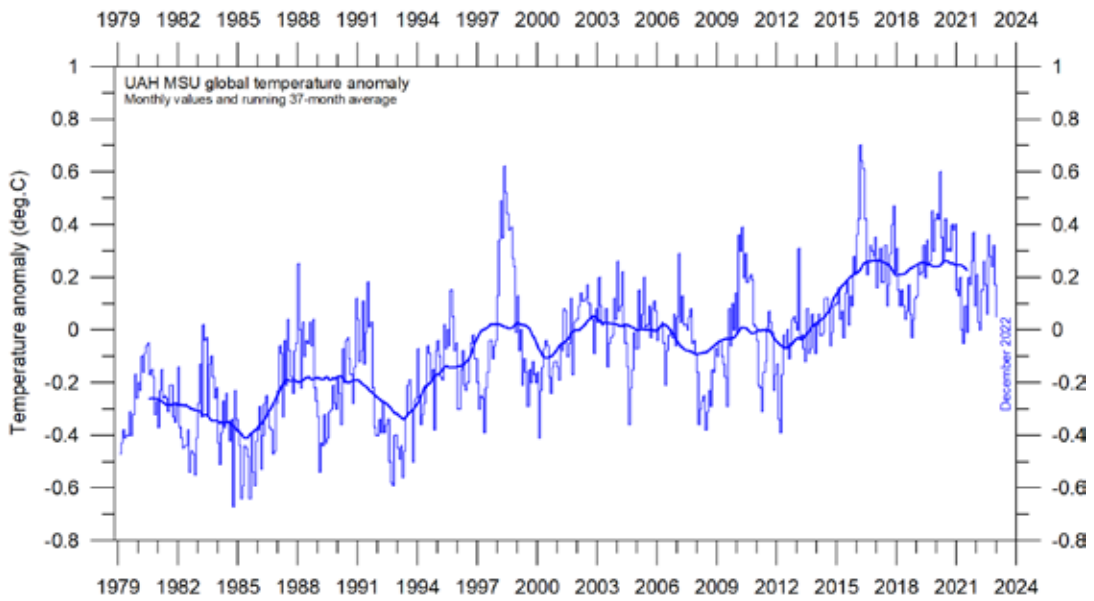


Lower Troposphere: monthly

Both satellite records of lower Troposphere temperatures clearly show a temperature spike associated with the 2015–16 El Niño, a subsequent gradual drop, followed by a new temperature spike due to the moderate 2019–20 El Niño. The latest development is a renewed temperature drop during the ongoing La Niña episode in the Pacific Ocean.

The pattern of temperature variation is similar for the two data series (Figures 3–5), but the overall temperature increase for 1979–2022 is larger for RSS than for UAH. Before the rather significant adjustment of the RSS series in 2017, the temperature increase was almost identical for the two data series.

(a) UAH



(b) RSS

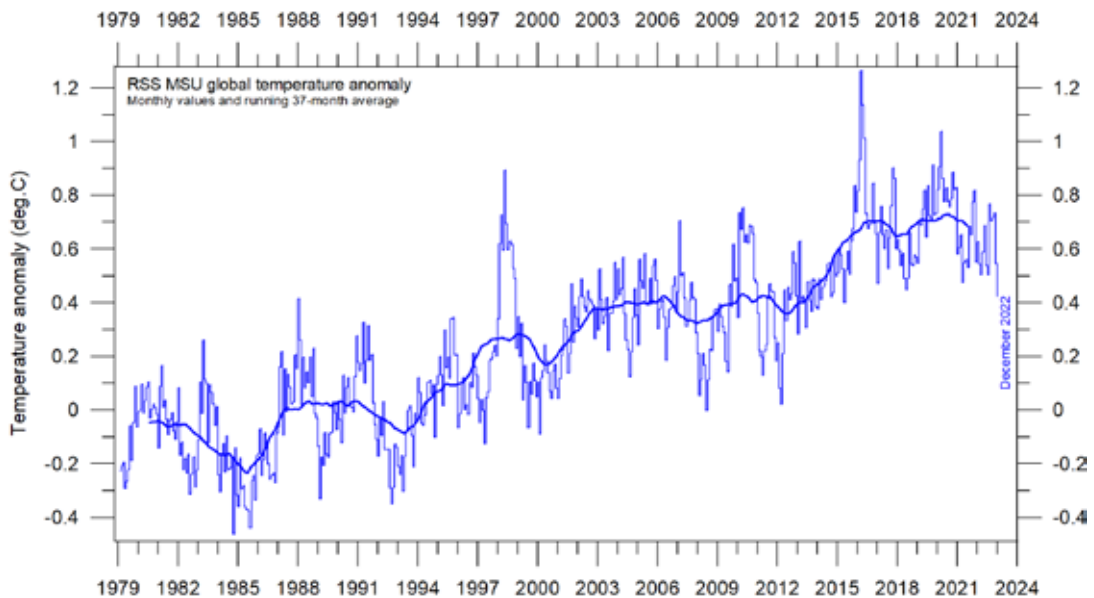
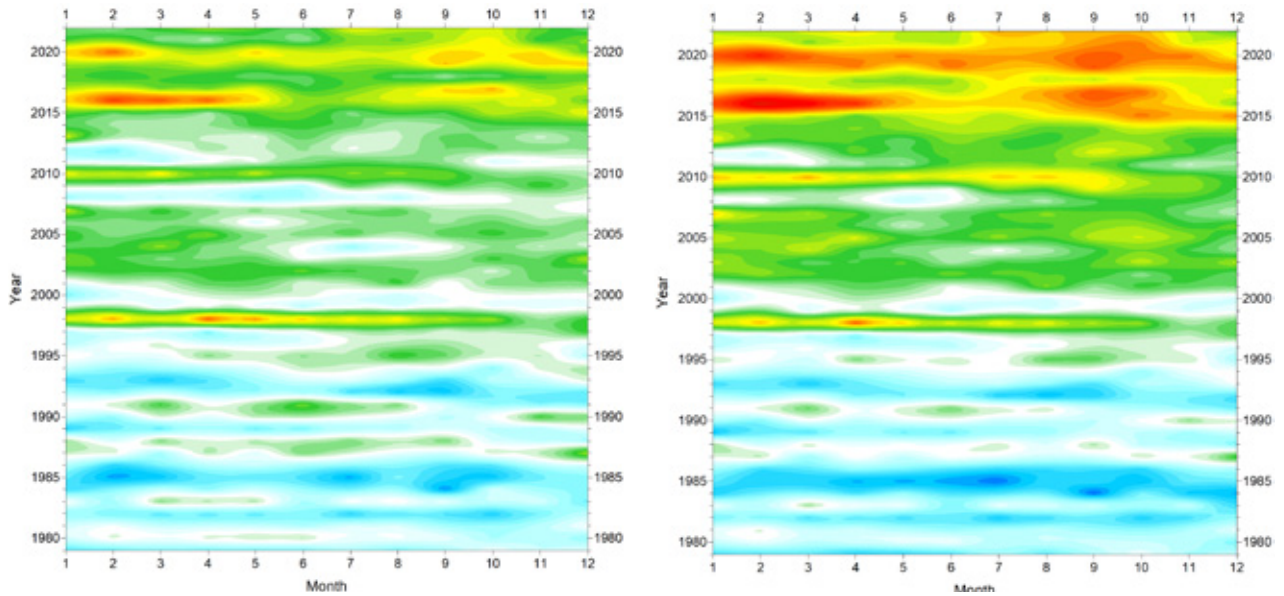


Figure 3: Global monthly average lower troposphere temperatures since 1979.

(a) UAH and (b) RSS. The thick line is the simple running 37-month average, nearly corresponding to a running 3-year average.



(a) UAH

(b) RSS

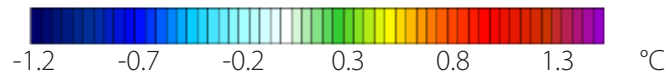


Figure 4: Temporal evolution of global lower troposphere temperatures since 1979.

Temperature anomaly versus 1979–2008. The effects of the El Niños of 1998, 2010 and 2015–2016 are clearly visible, as are the tendency for many El Niños to culminate during the Northern Hemisphere winter. As the different temperature databases are using different reference periods, the series have been made comparable by setting their individual 30-year average (1979–2008) to zero.

Lower Troposphere: annual means

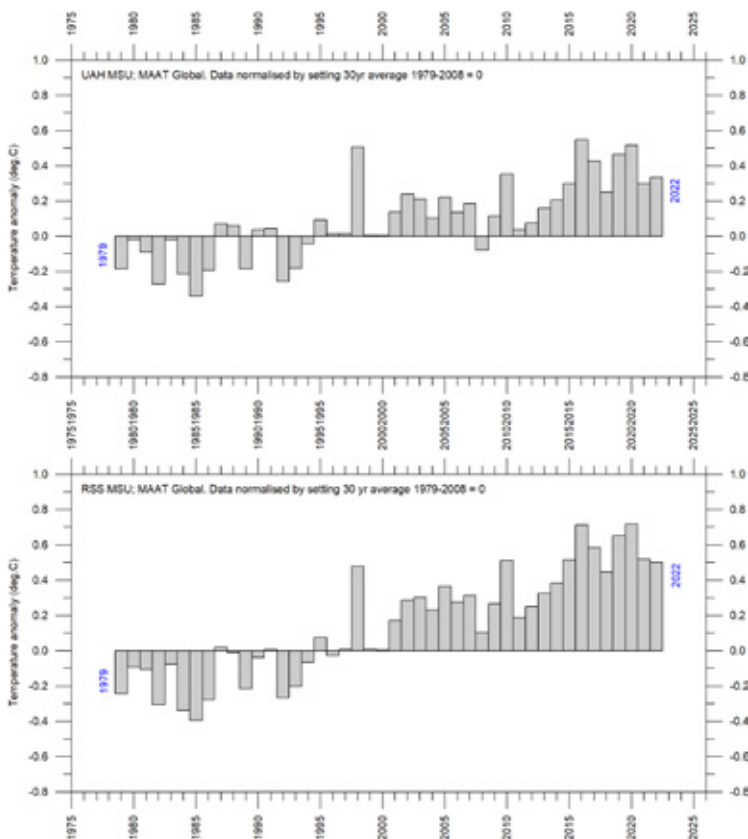


Figure 5: Global mean annual lower troposphere air temperatures since 1979.

Satellite data interpreted by the University of Alabama at Huntsville (UAH), and Remote Sensing Systems (RSS), both in the USA.

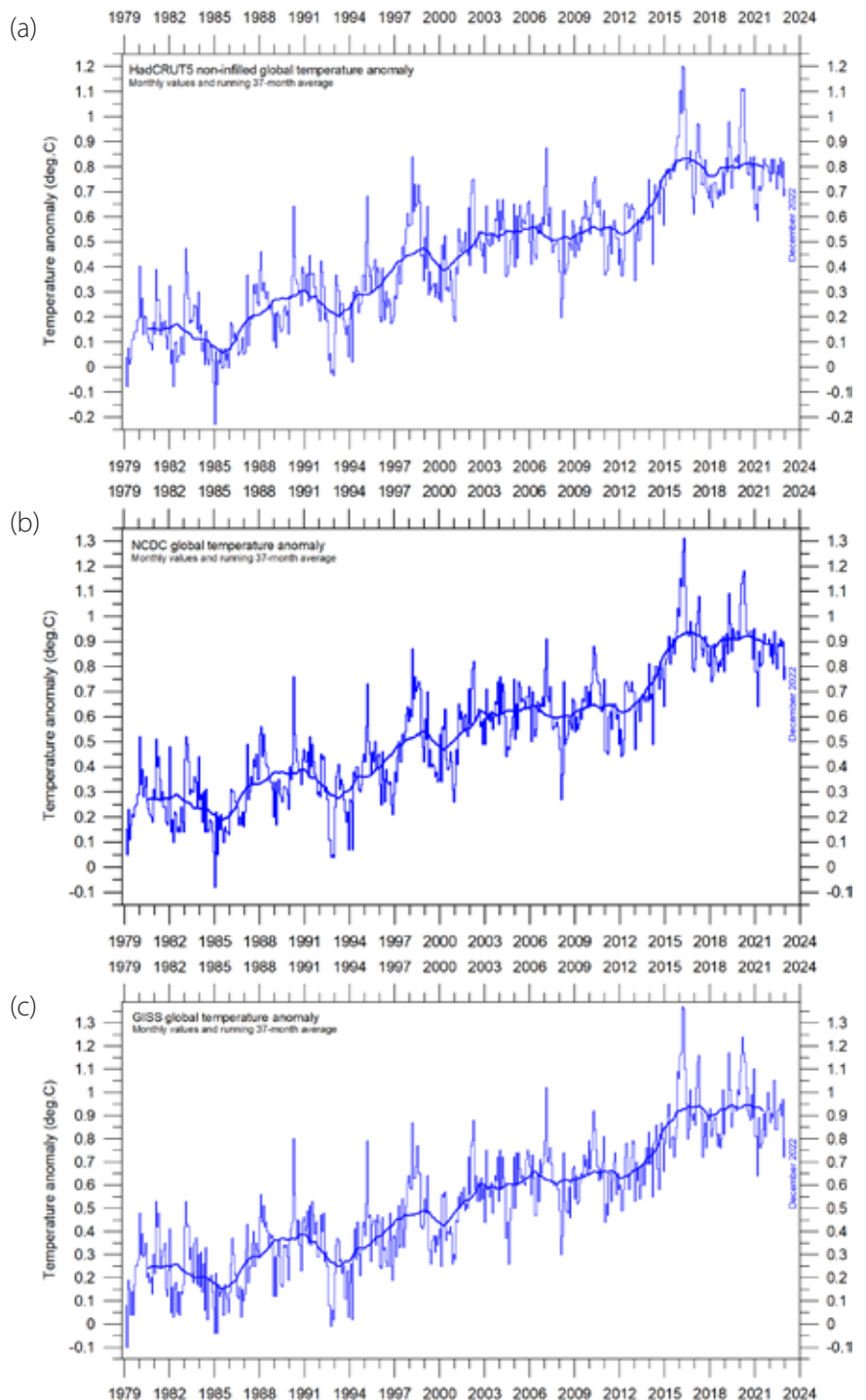
Surface: monthly

All three surface air temperature records clearly show the temperature spike associated with the 2015–16 El Niño, the subsequent temperature drop, a renewed temperature increase due to the 2019–20 El Niño, and the latest temperature decrease due to the ongoing La Niña episode (Figure 6).

All three surface records, however, confirm that the recent major El Niño episode culminated in early 2016, that there was a subsequent gradual turning back towards pre-2015 conditions, a renewed increase in 2019–20 and a subsequent temperature decrease. These developments are also seen in Figure 7.

Figure 6: Global mean monthly surface air temperatures since 1979.

(a) HadCRUT5 (b) NCDC (c) GISS. The thick line is the simple running 37-month average, nearly corresponding to a running 3-year average.



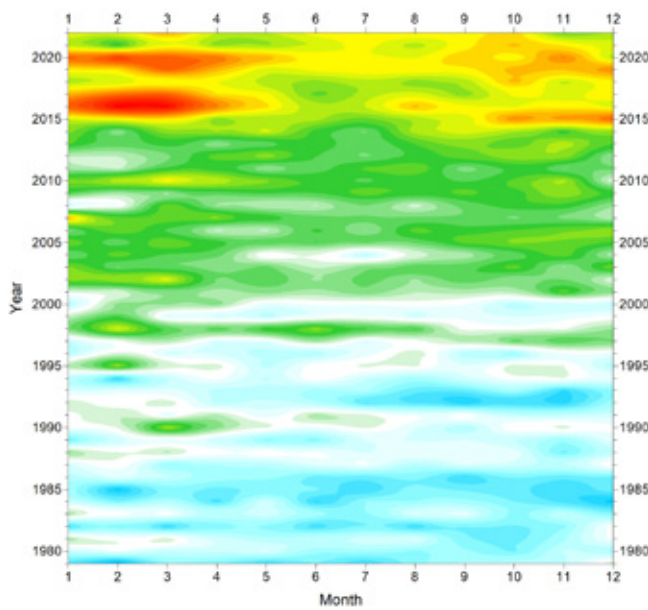
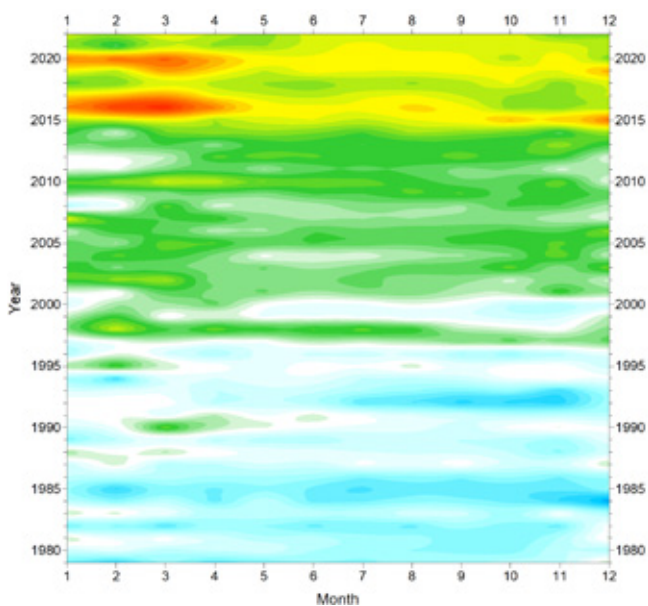
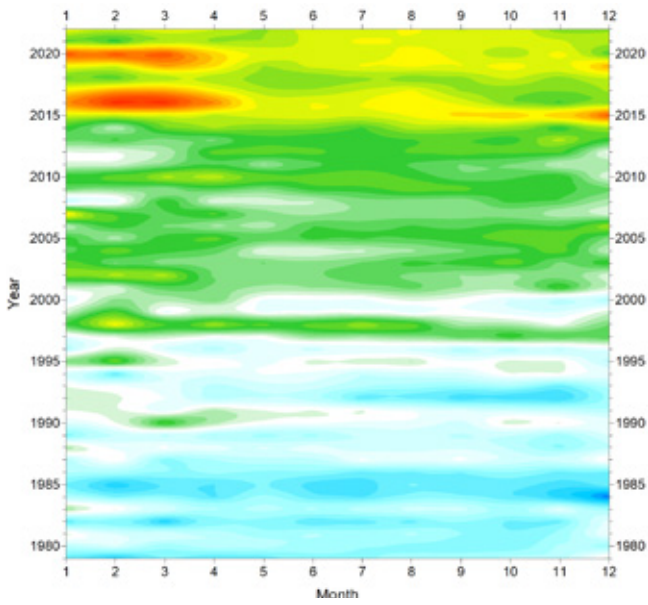
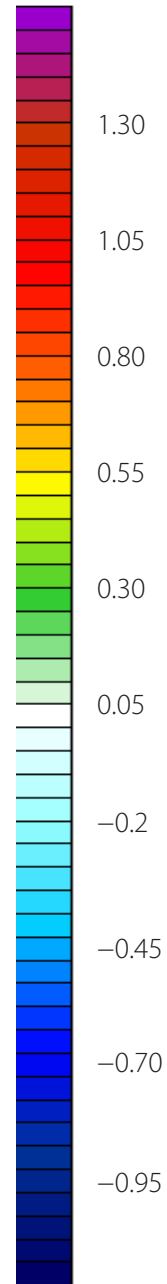


Figure 7: Temporal evolution of global mean monthly surface air temperatures.

(a) HadCRUT (b) NCDC (c) GISS. Temperature anomaly (°C) versus 1979–2008.

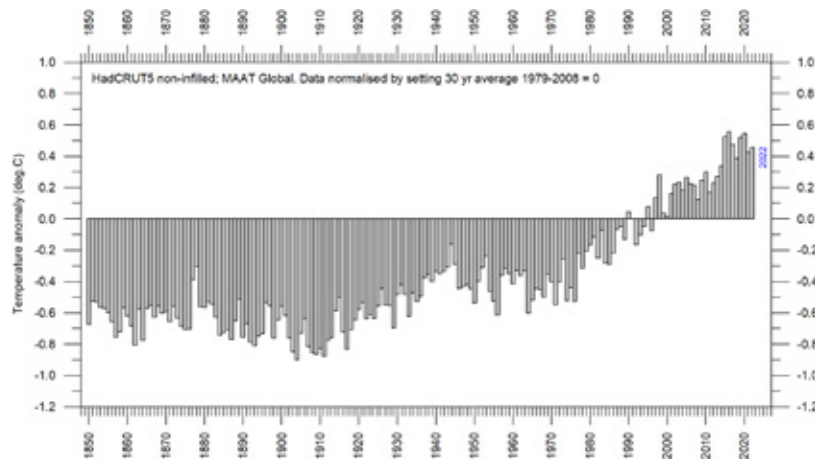
Temperature anomaly (°C)



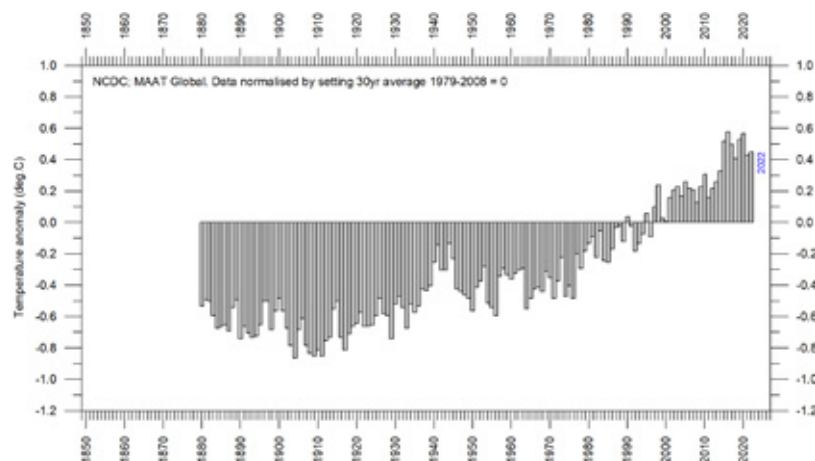
Surface: annual means

All three average surface air temperature estimates show 2022 as part of a declining trend since 2016 (Figure 8). The year 2022 was influ-

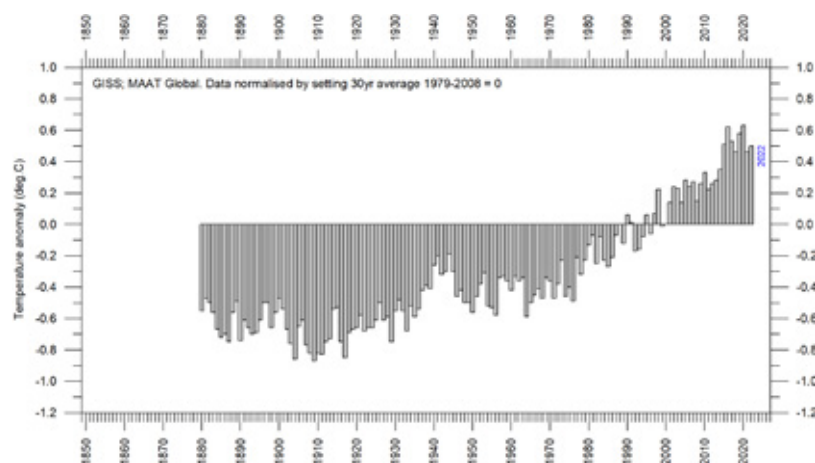
enced by a La Niña episode playing out in the Pacific Ocean (see Figure 22).



(a) HadCRUT



(b) NCDC



(c) GISS

Figure 8: Global mean annual surface air temperatures. (a) HadCRUT (b) NCDC (c) GISS temperature anomaly (°C) versus 1979–2008.

Error, consistency and quality

According to the various air temperature datasets, 2022 was a warm year, when considering the entire record since 1850/1880/1979.

The surface records represent a blend of sea-surface data, collected by moving ships or by other means, and data from land stations, of partly unknown quality and unknown representativeness for their region. Many of the land stations have also been moved geographically during their period of operation, instrumentation has been changed, and most have been influenced by ongoing changes in their surroundings (vegetation, buildings, and so on).

The satellite temperature records have their own problems, but these are generally of a more technical nature and therefore are probably easier to rectify. In addition, the sampling by satellites is more regular and complete on a global basis than for the surface records. It is also important to note that the sensors on satellites measure temperature directly, by emitted radiation, while most modern surface temperature measurements are indirect, using electronic resistance.

All temperature records are affected by at least three different sources of error, which differ between the individual station records used for calculation of a global average temperature estimate. 1) The *accuracy* is the degree of closeness of measurements to the actual (true) values. 2) The *precision* is the degree to which repeated measurements under unchanged conditions show an identical value, true or not. In addition, we have 3) the measurement *resolution*, which is the smallest change in temperature that produces a response in the instrument used for measurement. Combined, these represent the *margin of error* for temperature records. The margin of error has been intensively discussed over time and is probably at least $\pm 0.1^{\circ}\text{C}$ for surface air temperature datasets, and possibly higher. This often makes it statistical impossible to classify any year as representing a temperature record, as several other years may be within the $\pm 0.1^{\circ}\text{C}$ range of the value considered.

In addition, two other issues relating to the margin of error for surface records have not

been so widely discussed: First, as an example, it will not be possible to conclude much about the actual value of the December 2022 global surface air temperature before March–April 2023, when data not yet reported (in January 2023) are finally incorporated in the surface air temperature databases. This is what might be described as the effect of *delayed reporting*. Secondly, surface air temperature records often display *administrative changes* over time, which makes it even more difficult to draw conclusions about the significance of any recently reported monthly or annual surface air temperature.

The administrative issue arises from the apparently perpetual changes of monthly and annual values made to temperature databases. This means that the value reported today as the average global temperature for previous years will later change due to ongoing administrative ‘corrections’. These changes appear to have little or nothing to do with delayed reporting of missing data: particularly with the GISS and NCDC databases, changes are made to monthly temperatures for periods far back in time, even before the year 1900, for which the possibility of reporting delays is exceedingly small. Most likely, such administrative changes are the result of alterations in the way average monthly values are calculated by the various databases, in an attempt to enhance the resulting record.

As an example, Figure 9 shows the accumulated effect since May 2008 of such administrative changes in the GISS global surface air temperature record, extending back to 1880, although any of the other datasets could be used instead. The overall net effect of the administrative changes introduced in the GISS record since May 2008 is a warming of the early and modern part of the record and cooling of the period in between, roughly from 1900 to 1970. Several of the net changes introduced since 2008 are quite substantial, ranging from about $+0.20$ to -0.20°C .

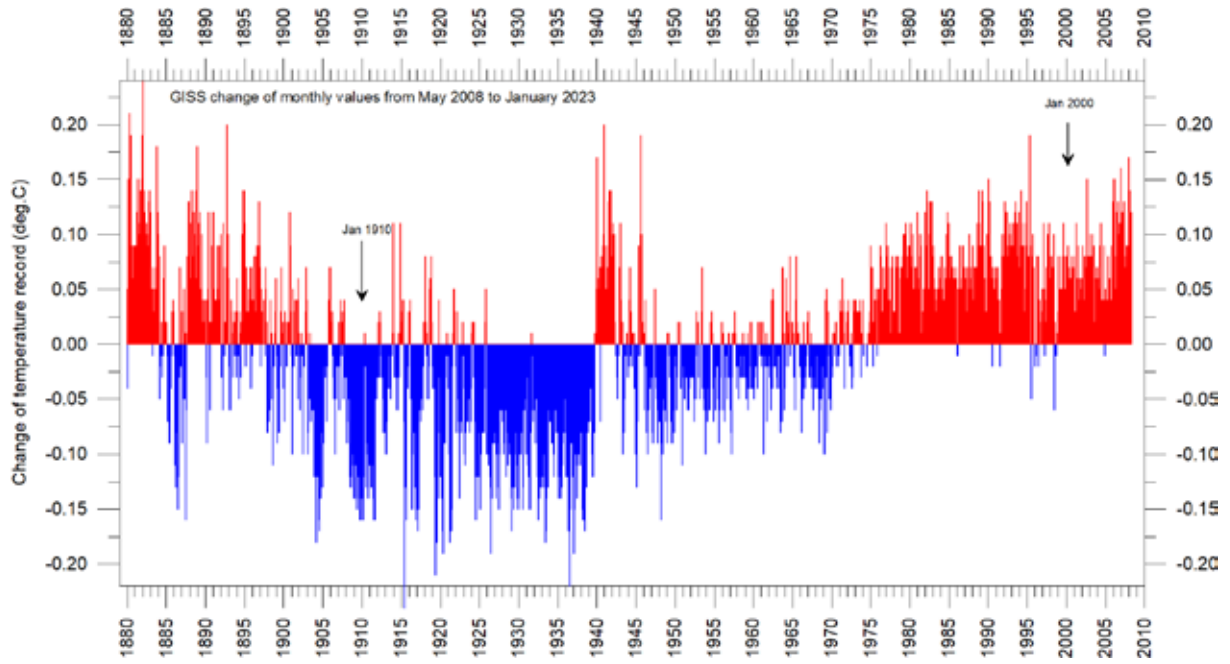


Figure 9: Adjustments since 17 May 2008 in the GISS surface temperature record.

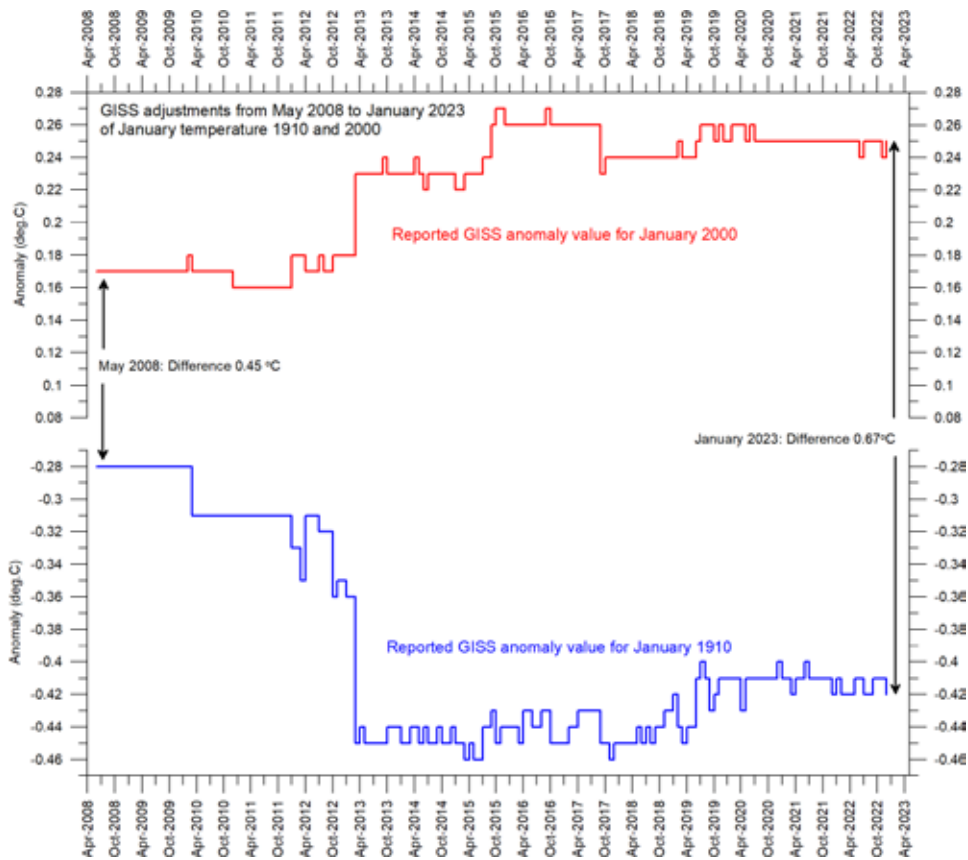


Figure 10: Adjustments made since May 2008 to GISS anomalies for the months January 1910 and January 2000.

To illustrate the effect in a different way, Figure 10 shows how the global surface air temperature for January 1910 and January 2000 (months indicated in Figure 15) has changed since May 2008, again exemplified by the GISS record. The GISS administrative uplift has increased apparent warming of global surface air temperatures between January 1910 and January 2000, from 0.45 (as reported in May 2008) to 0.67°C (as reported in January 2023). This represents an about 49% increase over this period, meaning that just about half of the apparent global temperature increase from January 1910 to January 2000 (as reported by GISS in January 2023) is due to administrative changes to the original data since May 2008. Clearly such changes are important when evaluating the overall quality of various temperature records,

along with other standard sources of error. In fact, the magnitude of administrative changes may exceed the formal margin of error.

For obvious reasons, as the past does not change, any record undergoing continuing changes cannot describe the past correctly all the time. Frequent and large corrections in a database unavoidably signal a fundamental uncertainty about the correct values. Nevertheless, everybody interested in climate science should gratefully acknowledge the efforts put into maintaining the different databases referred to in the present report. At the same time, however, it is also important to realise that all temperature records cannot be of equal scientific quality. The simple fact that they to some degree differ shows that they cannot all be completely correct.



Surface versus lower Troposphere

In general, there is fair agreement between the average of the surface and satellite records, as shown by Figure 11. However, before the major adjustment of the RSS satellite record in 2017, this was different, with the average of surface records drifting in warm direction, compared to the average of satellite records. Again, this illustrates the importance of ongoing changes of the individual temperature records.

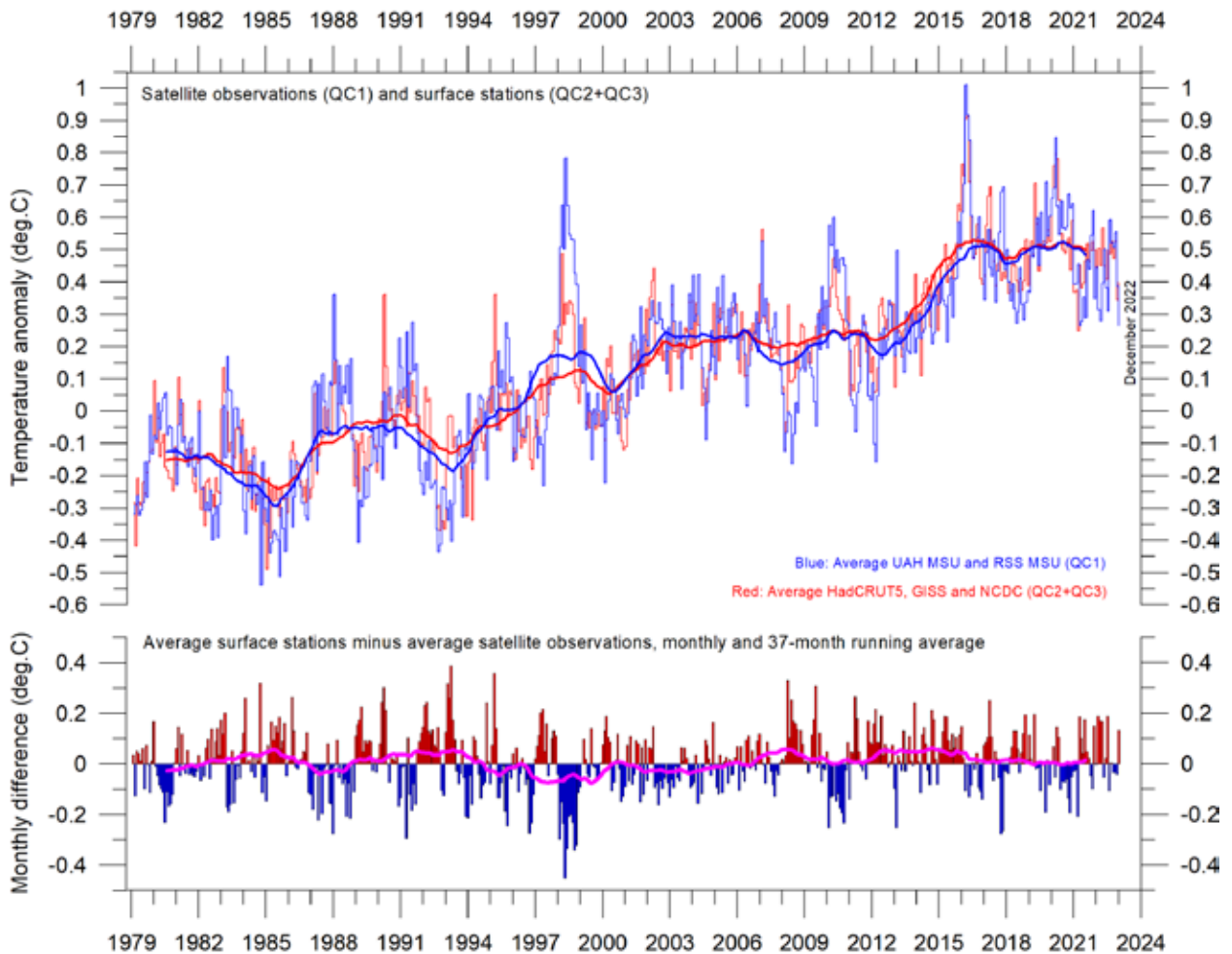


Figure 11: Surface temperatures versus lower Troposphere temperatures.

Average of monthly global surface air temperature estimates (HadCRUT, NCDC and GISS) and satellite-based lower Troposphere temperature estimates (UAH and RSS). The thin lines indicate the monthly value, while the thick lines represent the simple running 37-month average, nearly corresponding to a running 3-year average. The lower panel shows the monthly difference between surface air temperature and satellite temperatures. As the base period differs for the different temperature estimates, they have all been normalised by comparing to the average value of 30 years from January 1979 to December 2008.

Lower Troposphere: land versus ocean

Since 1979, the lower Troposphere has warmed considerably more over land than over the oceans (Figure 12). There may be several reasons for this, such as differences in heat capacity, and variations in incoming solar radiation, cloud cover and land use.

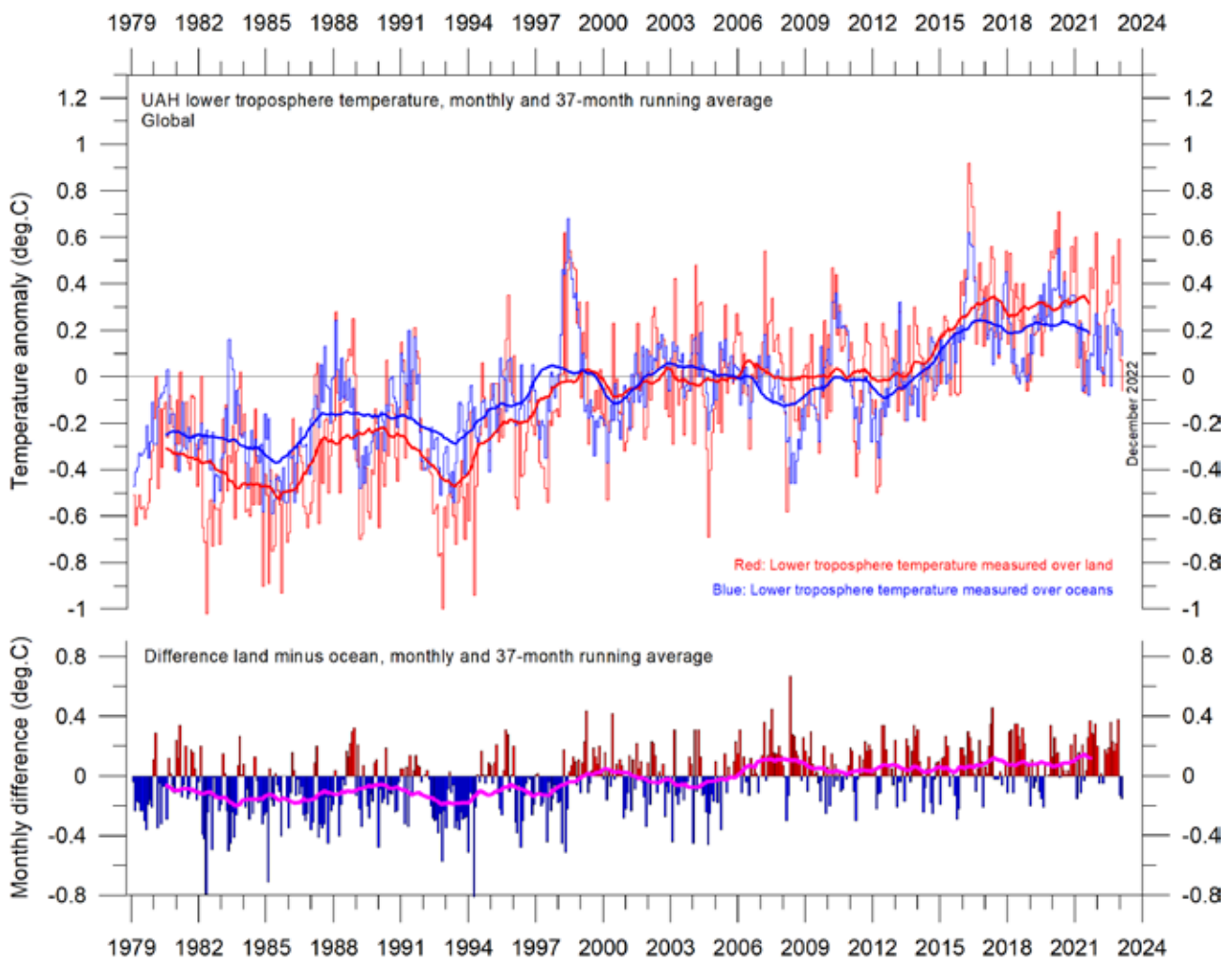


Figure 12: Lower Troposphere temperatures over land and ocean

Global monthly average lower troposphere temperature since 1979 measured over land and oceans, shown in red and blue, respectively, according to University of Alabama at Huntsville (UAH), USA. The thin lines represent the monthly average, and the thick line the simple running 37-month average, nearly corresponding to a running 3-year average.

By altitude

Changes in the vertical temperature profile of the atmosphere are interesting. One reason is that increasing Tropospheric temperatures along with decreasing Stratospheric temperatures are two central features of the hypothesis ascribing global warming to human-induced atmospheric CO₂ increases.

The temperature variations recorded in the lowermost Troposphere are generally reflected at higher altitudes, up to about 10 km altitude, including many individual troughs and peaks, such as the El Niño induced temperature spike of 2015–16 (Figure 13)

At high altitudes, near the Tropopause, the

pattern of variations recorded lower in the atmosphere can still be recognised, but for the duration of the record (since 1979) there has been no clear trend towards higher or lower temperatures.

Higher in the atmosphere, in the Stratosphere, at 17 km altitude, two pronounced temperature spikes are visible before the turn of the century. Both can be related to major volcanic eruptions, as indicated in the diagram. Ignoring these, until about 1995 the Stratospheric temperature record shows a persistent and marked decline, ascribed by several scientists to the effect of heat being trapped by CO₂ in the

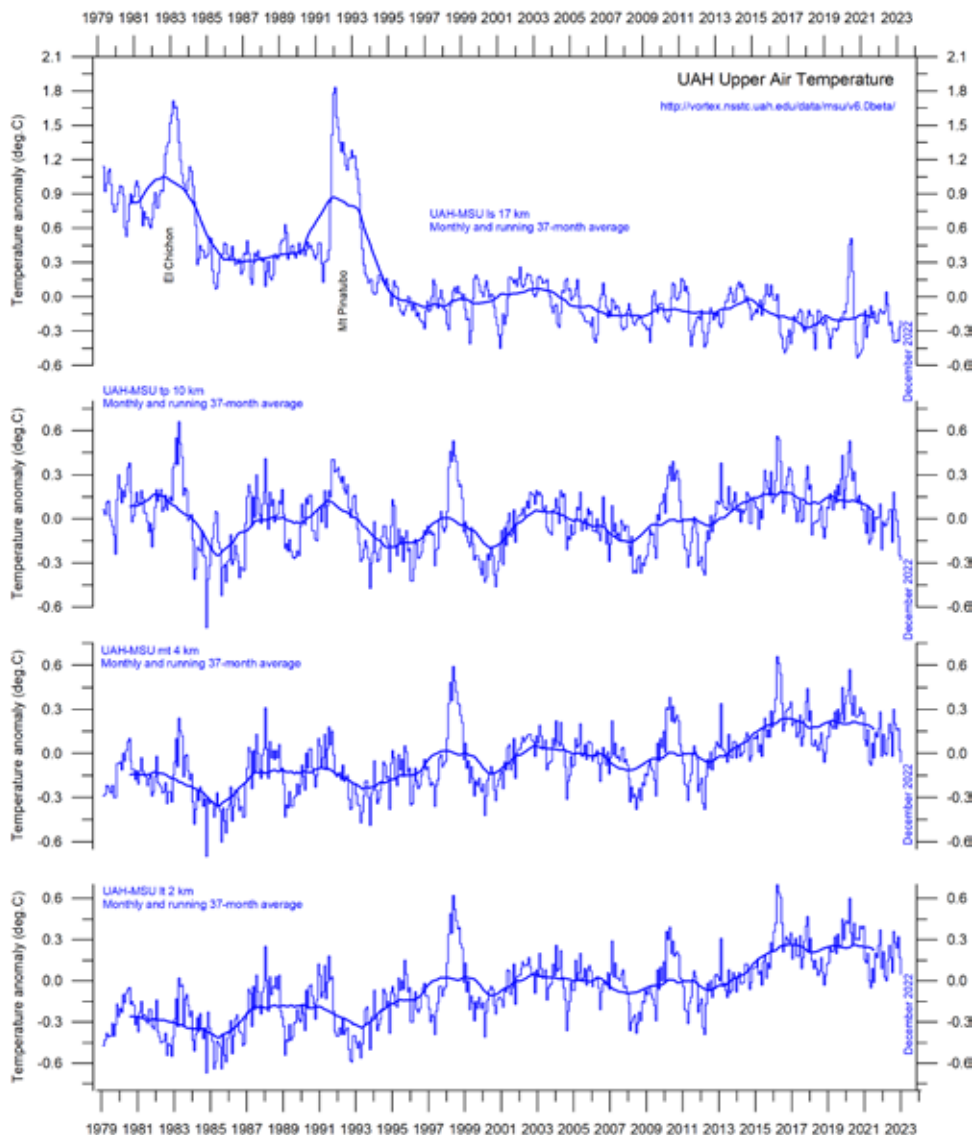


Figure 13: Temperature by altitude.

Global monthly average temperature in different altitudes according to University of Alabama at Huntsville (UAH), USA. The thin lines represent the monthly average, and the thick line the simple running 37-month average, nearly corresponding to a running 3-year average.

Troposphere below. However, the marked Stratospheric temperature decline essentially ends around 1995–96, and there has been a long temperature plateau since that time. In 2020, however, there was a marked, but short-lived,

temperature peak, rapidly followed by a drop in temperature of similar magnitude. Since the end of 2020, Stratospheric temperatures have essentially returned to pre-2020 levels.

Zonal air temperatures

Figure 14 shows that the ‘global’ warming experienced after 1980 has predominantly been a Northern Hemisphere phenomenon, and mainly played out as a marked step change between 1994 and 1999. This rapid temperature change was, however, influenced by the Mt Pinatubo eruption of 1992–93 and the 1997 El Niño episode.

The figure also reveals how the temperature effects of the strong equatorial El Niños of 1997 and 2015–16, as well as the moderate one in 2019, apparently spread to higher latitudes in both hemispheres, although with some delay. The effect was, however, mainly seen in the Northern Hemisphere, and only to lesser degree in the Southern Hemisphere. The recent temperature decrease in the tropics (20°N–20°S) since 2016 is noteworthy.

The figure also reveals how the tempera-

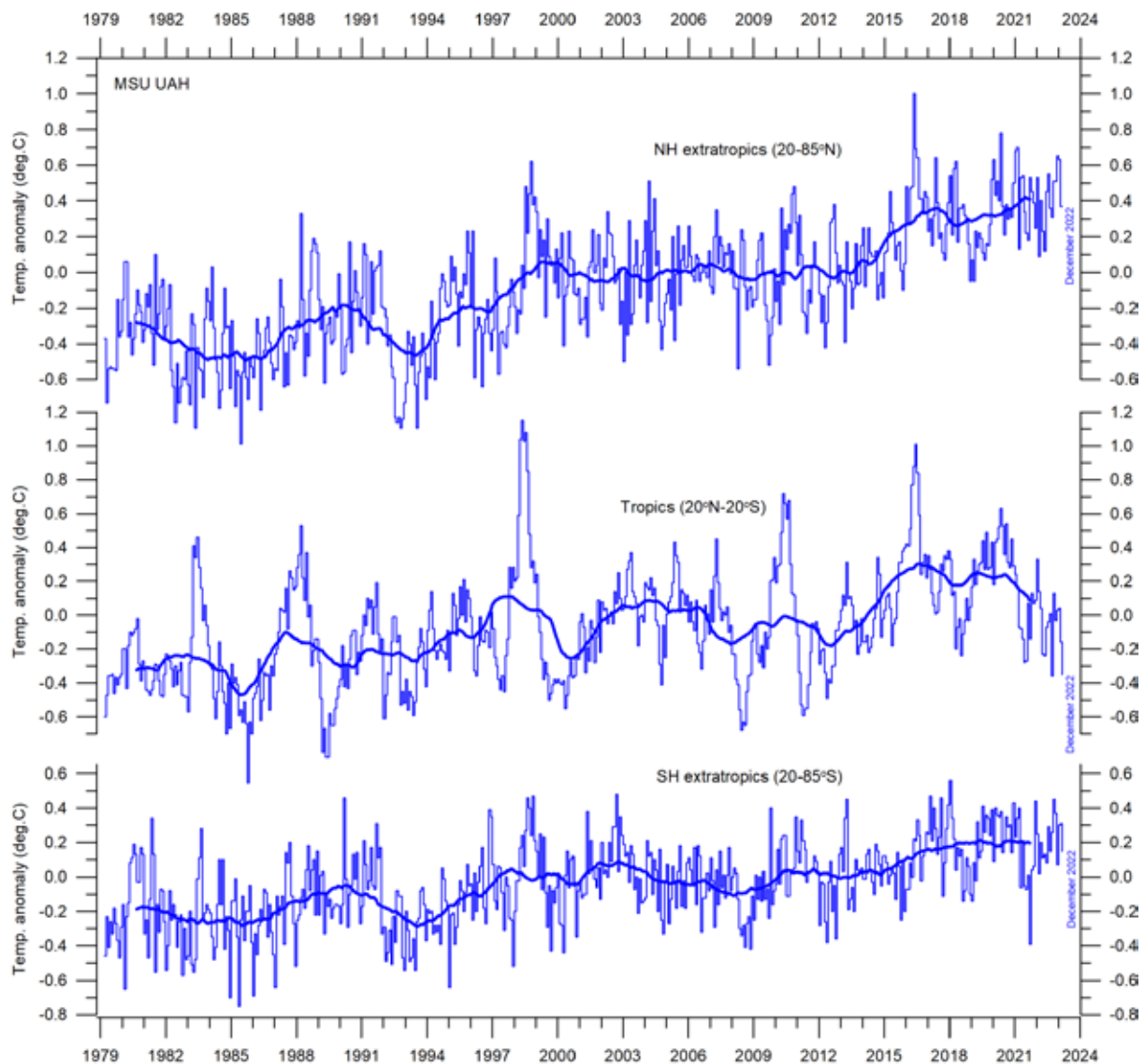


Figure 14: Zonal air temperatures.

Global monthly average lower troposphere temperature since 1979 for the tropics and the northern and southern extratropics, according to University of Alabama at Huntsville, USA. Thin lines: monthly value; thick lines: 3-year running mean.

Polar air temperatures

In the Arctic region, warming was rapid in the period 1994–96, but slower subsequently (Figure 15). In 2016, however, temperatures peaked for several months, presumably because of oceanic heat given off to the atmosphere during the El Niño of 2015–16 (see also Figure 22) and then advected to higher latitudes. A small temperature decrease has characterised the Arctic since 2016.

In the Antarctic region, temperatures have essentially remained stable since the onset of

the satellite record in 1979. In 2016–17, a small temperature peak, visible in the monthly record, might be interpreted as the subdued effect of the recent El Niño episode.

Arctic and Antarctic temperature peaks derived from El Niño episodes, as outlined above, are paradoxically due to heat ventilating out from the Pacific Ocean near the Equator. They therefore represent a process cooling the Earth, when considered in a broader context.

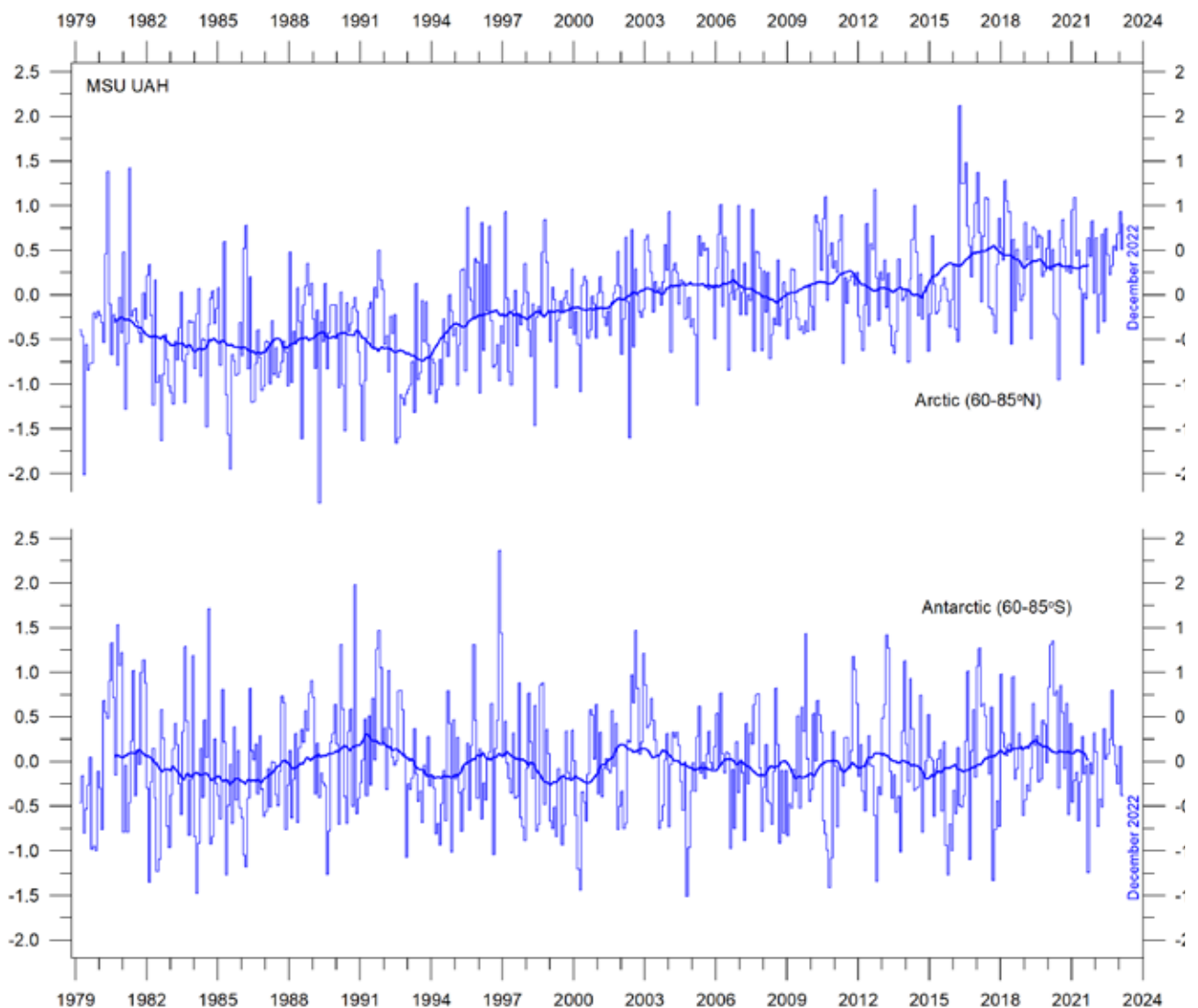


Figure 15: Polar temperatures

Global monthly average lower troposphere temperature since 1979 for the North and South Pole regions, according to University of Alabama at Huntsville (UAH), USA. Thick lines are the simple running 37-month average.

2. Atmospheric greenhouse gases

Water vapour

Water vapour (H_2O) is the most important greenhouse gas in the Troposphere. The highest concentration is found within a latitudinal range from $50^\circ N$ to $60^\circ S$. The two polar regions of the Troposphere are comparatively dry. H_2O is a much more important greenhouse gas than CO_2 , both because of its absorption spectrum and its higher concentration.

Figure 16 shows the specific atmospheric humidity to be stable or slightly increasing up to about 4–5 km altitude. At higher levels in the Troposphere (about 9 km), the specific humidity has been decreasing for the duration of the

record (since 1948), but with shorter variations superimposed on the falling trend. A Fourier frequency analysis (not shown here) suggests these changes are influenced, not only by annual variations, but also by a cycle of about 35-years' duration.

The overall decrease since 1948 in specific humidity at about 9 km altitude is notable, as this altitude roughly corresponds to the level where the theoretical temperature effect of increased atmospheric CO_2 is expected initially to play out.

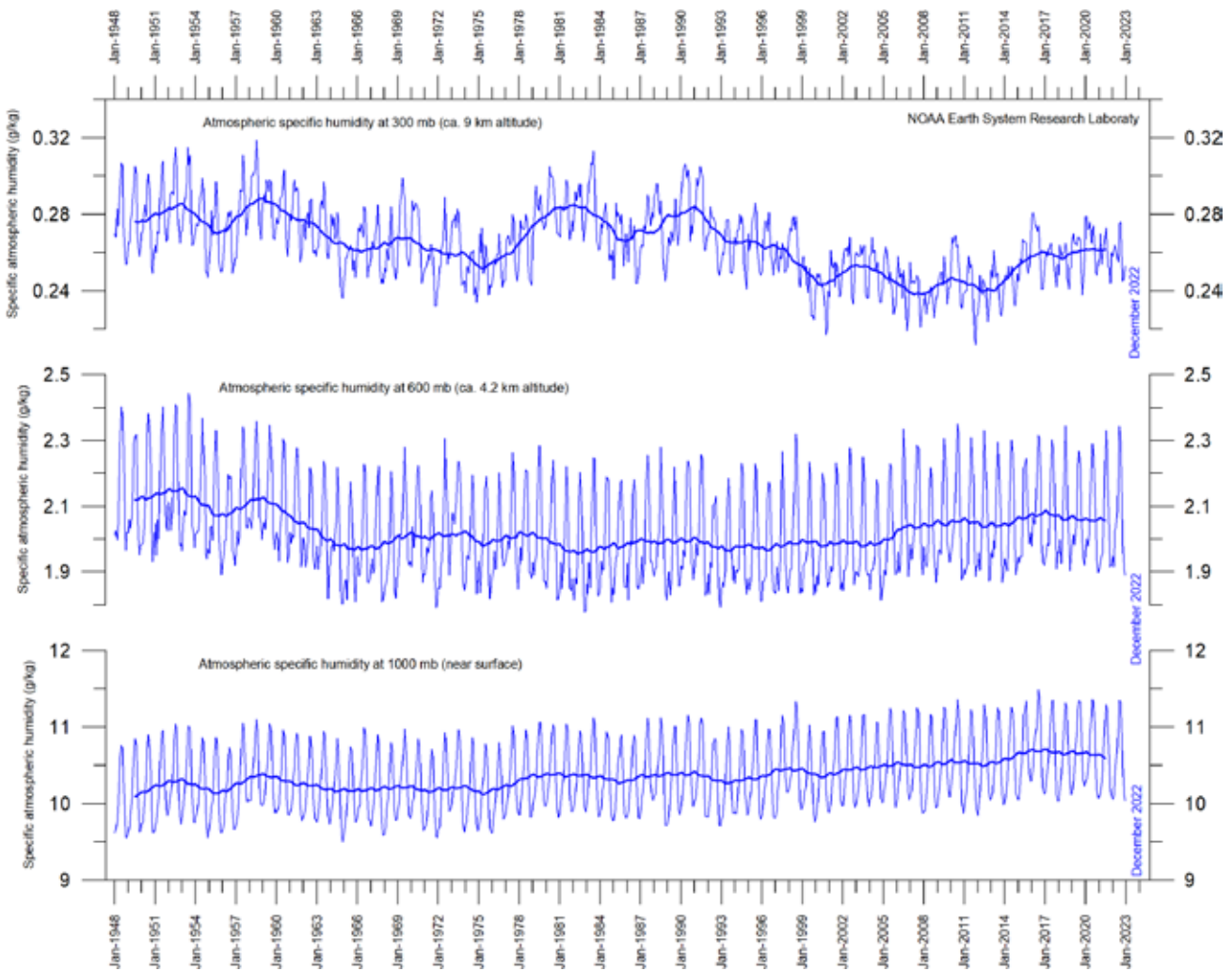


Figure 16: Humidity.

Specific atmospheric humidity (g/kg) at three different altitudes in the Troposphere since January 1948. The thin blue lines show monthly values, while the thick blue lines show the running 37-month average (about 3 years). Data source: Earth System Research Laboratory (NOAA).

Carbon dioxide

Carbon dioxide (CO₂) is an important greenhouse gas, although less important than H₂O. Since 1958, there has been an increasing trend in its atmospheric concentration, with an annual cycle superimposed. At the end of 2021, the amount of atmospheric CO₂ was close to 419 parts per million (ppm; Figure 17). CO₂ is generally considered as a relatively well-mixed gas in the Troposphere.

The 12-month change in Tropospheric CO₂ has been increasing from about +1 ppm/year in the early part of the record, to about +2.6 ppm/year towards the end of the record (Figure 18). A Fourier frequency analysis (not shown here)

shows the 12-month change of Tropospheric CO₂ to be influenced especially by a significant periodic variation of 3.6-years' duration. There is no visible effect of the global COVID-19 lockdown 2020–2021 in the amount of atmospheric CO₂.

It is informative to consider the variation of the annual change rates of atmospheric CO₂, and global air and sea-surface temperatures (Figure 19). All three rates clearly vary in concert, but sea-surface temperatures are a few months ahead of the global temperature, and 11–12 months ahead of atmospheric CO₂. Important changes apparently originate at the sea surface.

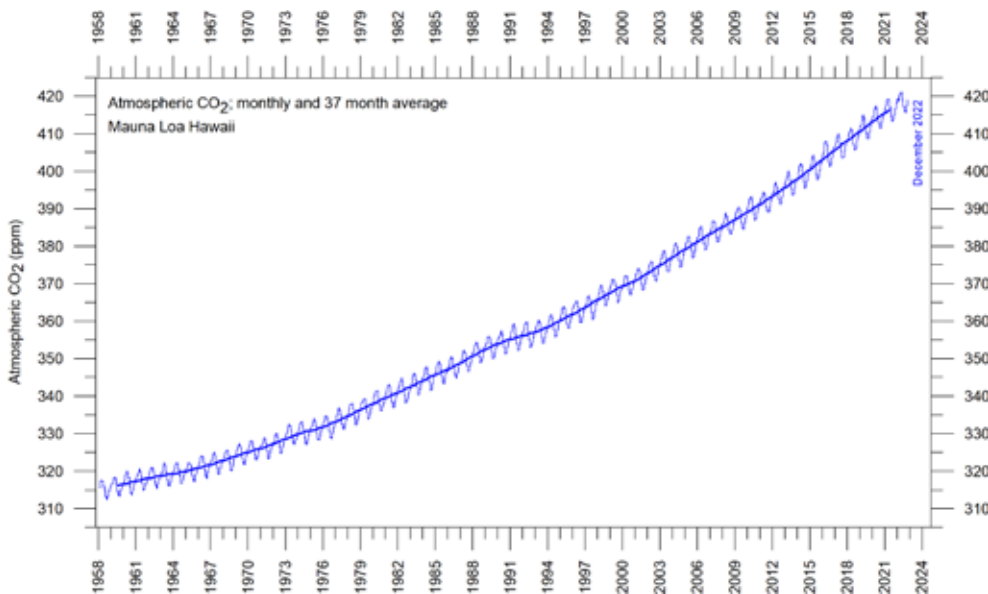


Figure 17: The Mauna Loa CO₂ record

Thin lines: monthly value;
thick lines: 37-month running mean.

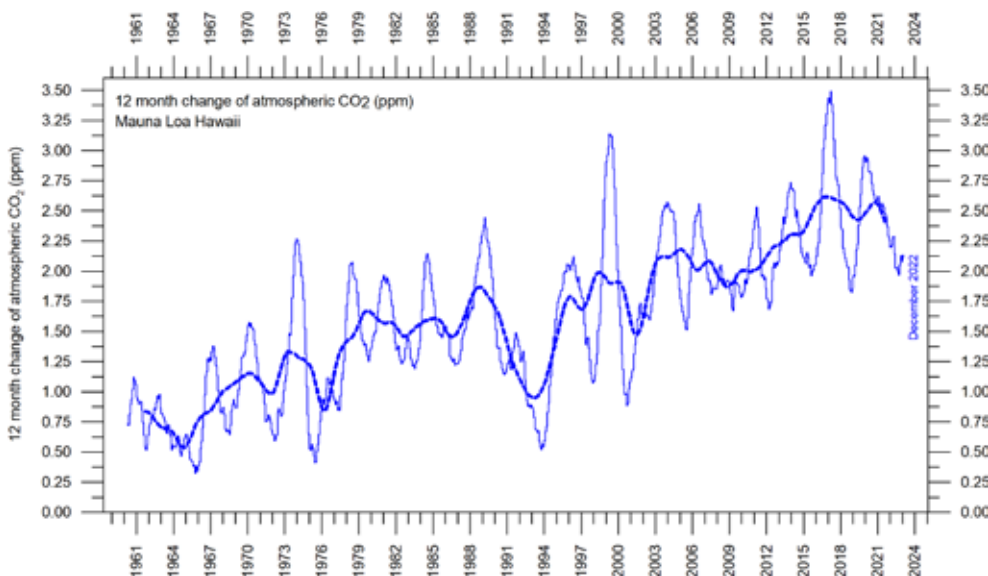


Figure 18: Annual CO₂ change

Difference of two
12-month averages. Thin
lines: monthly value; thick
lines: 3-year running mean.

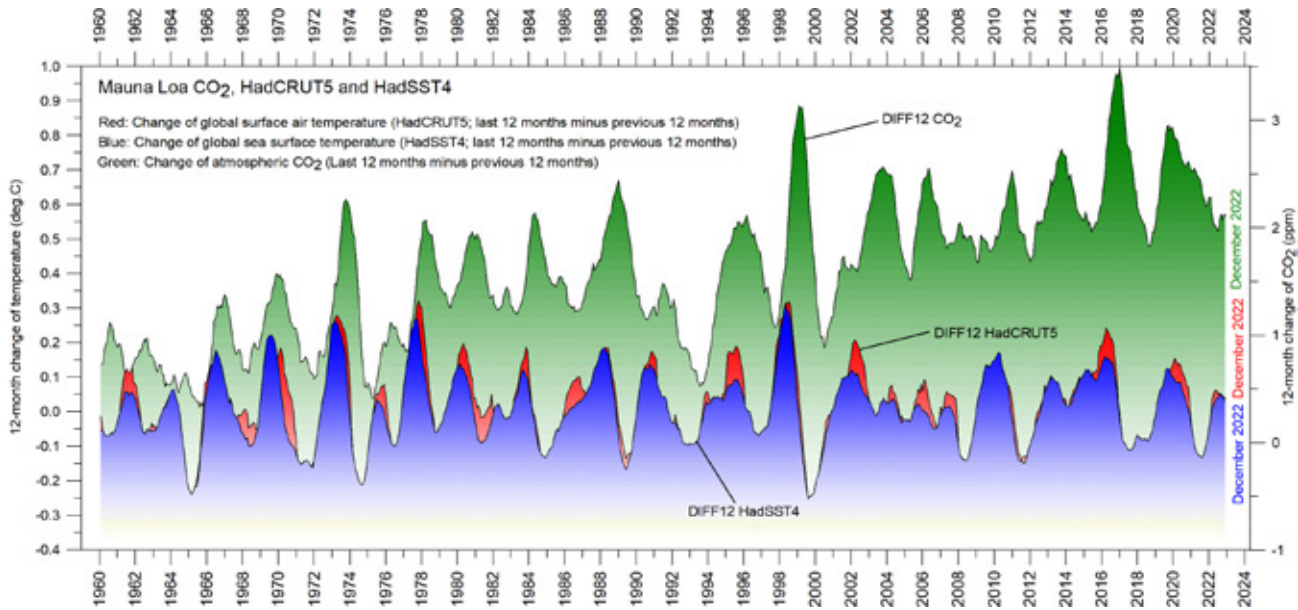


Figure 19: Correlation of carbon dioxide concentrations and temperature records.

Annual (12-month) change of global atmospheric CO₂ concentration (Mauna Loa; green), global sea surface temperature (HadSST4; blue) and global surface air temperature (HadCRUT5; red). All graphs are showing monthly values of DIFF12, the difference between the average of the last 12 months and the average for the previous 12 months for each data series.

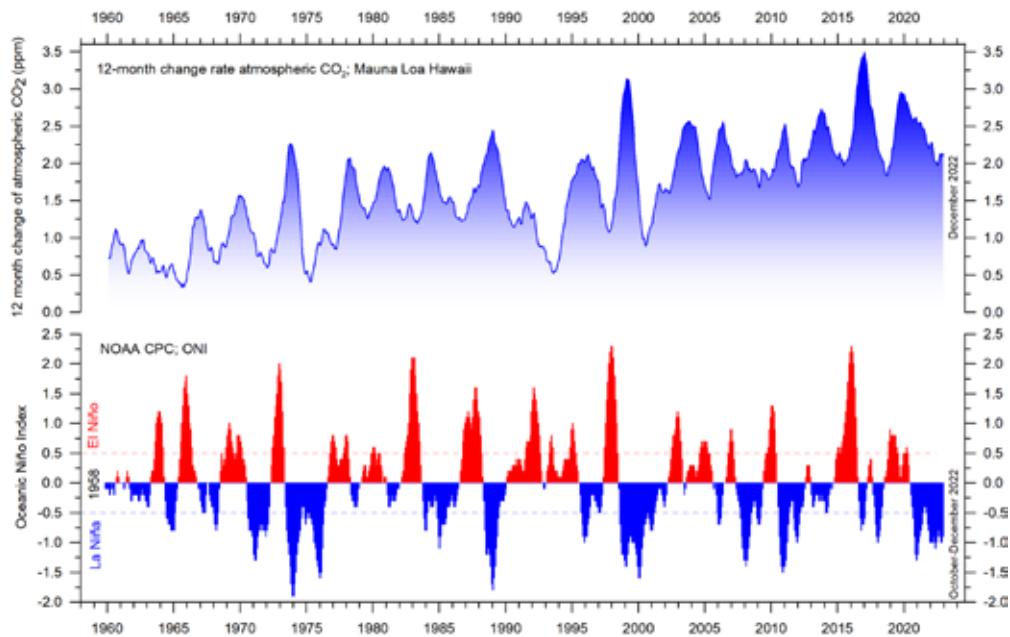


Figure 20: CO₂ growth and El Niño and La Niña episodes

Visual association between annual growth rate of atmospheric CO₂ (upper panel) and Oceanic Niño Index (lower panel).

Figure 20 shows the annual change of atmospheric CO₂ and its association with La Niña and El Niño episodes, emphasising the impor-

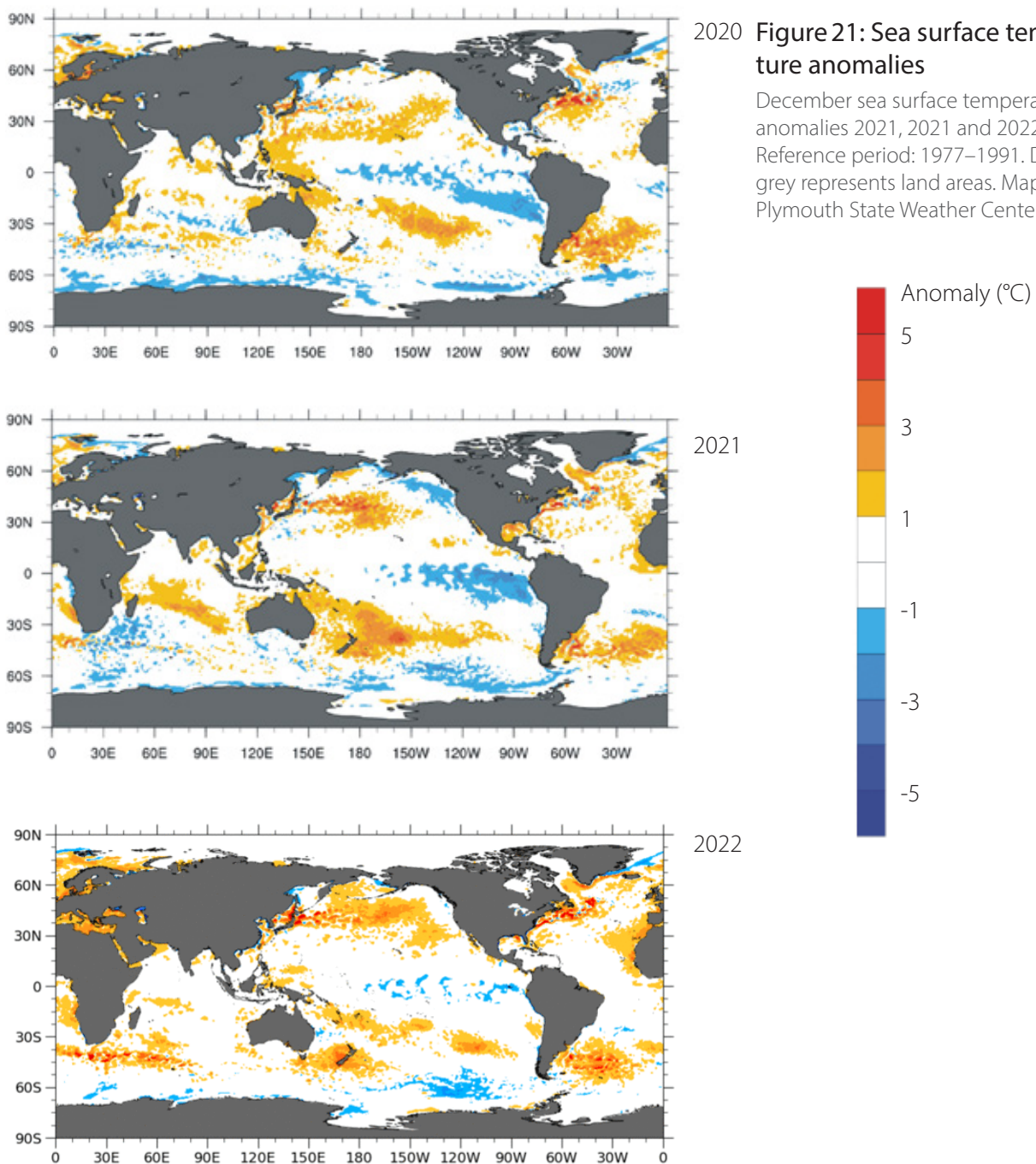
tance of ocean dynamics for understanding changes in atmospheric CO₂.

3. Ocean temperatures

Recent surface temperature anomalies

The three maps in Figure 21 show the moderate La Niña characterising much of 2020 and 2021, and its somewhat subdued effects at the end of 2022. Figure 22 shows all El Niño and La Niña episodes since 1950. The 2015–16 El Niño is among the strongest since the beginning of the record in 1950, and matches the global tem-

perature peak in 2016 (Figures 6, 7, and 12–14). Considering the entire record, however, recent variations in El Niño and La Niña episodes do not appear abnormal.



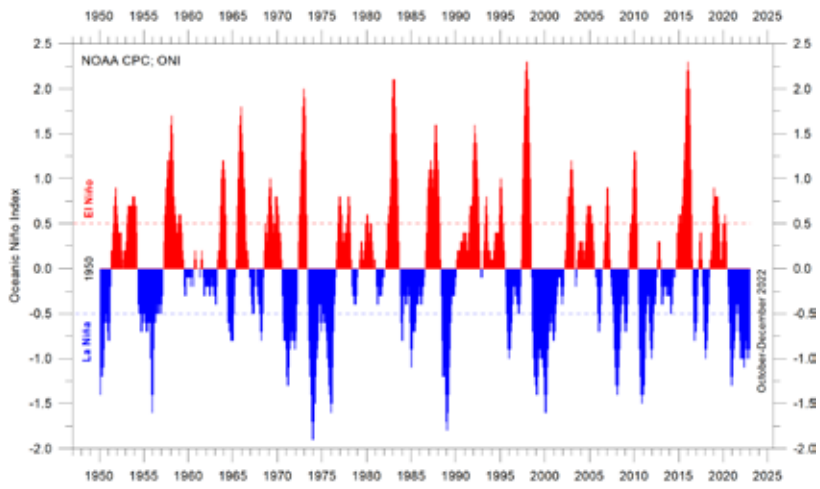


Figure 22: The El Niño index

Warm and cold episodes for the Oceanic Niño Index (ONI), defined as 3-month running mean of ERSST.v5 SST anomalies in the Niño 3.4 region (5°N–5°S, 120°–170°W). Anomalies are centred on 30-year base periods updated every 5 years.



By latitude

Based on observations by Argo floats (Roemich and Gilson 2009) the global summary diagram above (Figure 23) shows that, on average, the temperature of the global oceans down to 1900 m depth has been increasing since about 2010. It can also be seen that this increase since 2013 is predominantly due to oceanic changes

occurring near the Equator, between 30°N and 30°S. In contrast, for the circum-Arctic oceans, north of 55°N, depth-integrated ocean temperatures have been decreasing since 2011. Near the Antarctic, south of 55°S, temperatures have essentially been stable. At most latitudes, a clear annual rhythm is seen to play out.

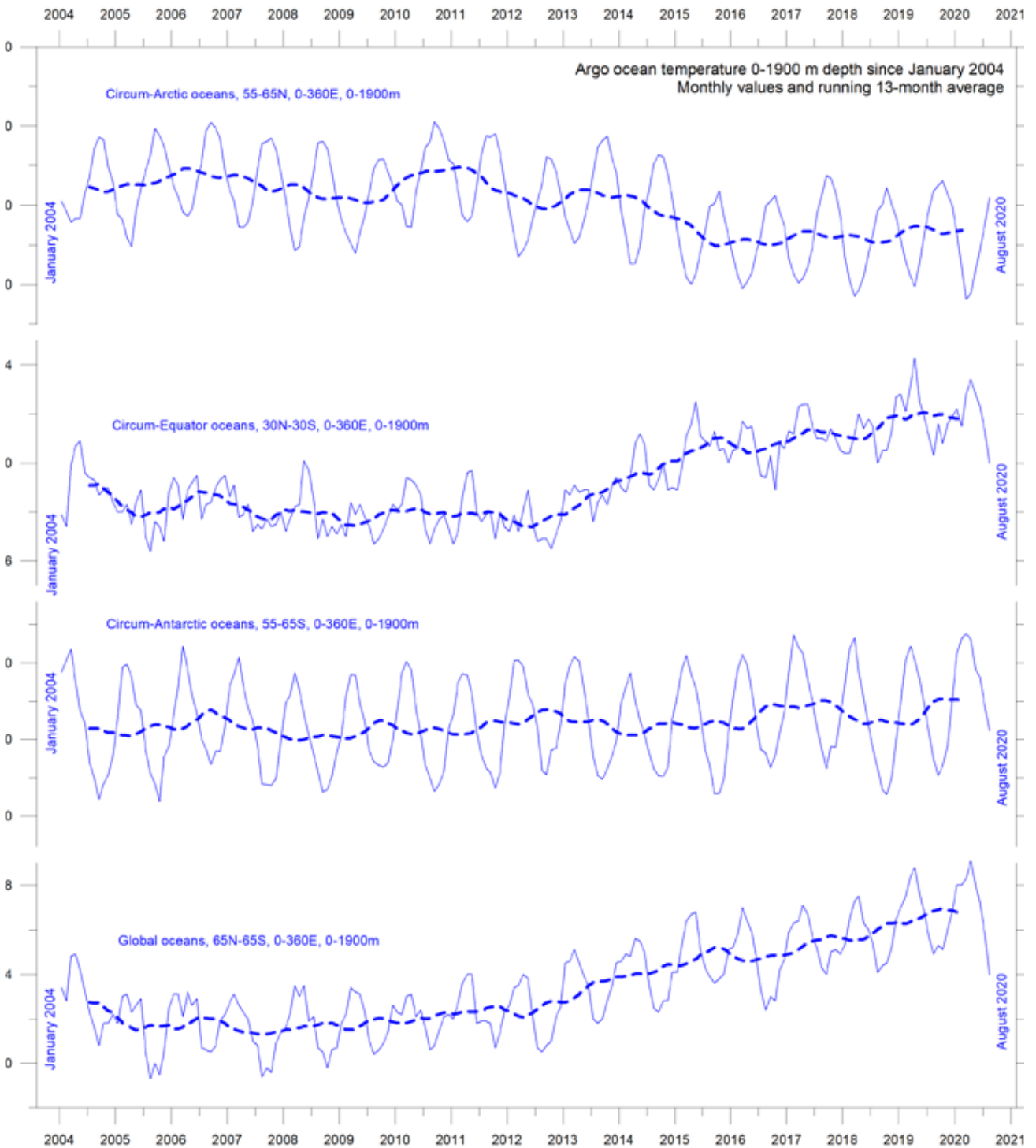


Figure 23: Ocean temperatures to 1900 m

Average ocean temperatures January 2004–August 2020 at 0–1900 m depth in selected latitudinal bands, using Argo data. The thin line shows monthly values, and the thick dotted line shows the running 13-month average. Source: Global Marine Argo Atlas.

By depth

Figure 24 displays global average oceanic temperatures at different depths. An annual rhythm can be traced to about 100 m depth. In the uppermost 100 m, temperatures have increased since about 2011. At 200–400 m depth, temperatures have exhibited little change during the observational period.

For depths below 400 m, however, temperatures have increased over the observa-

tional period. Interestingly, the data suggests that this increase commenced at 1900 m depth in around 2009, and from there has gradually spread upwards. At 600 m depth, the present temperature increase began around 2012; that is, about three years later than at 1900 m depth. The timing of these changes shows that average temperatures in the upper 1900 m of the oceans are not only influenced by conditions

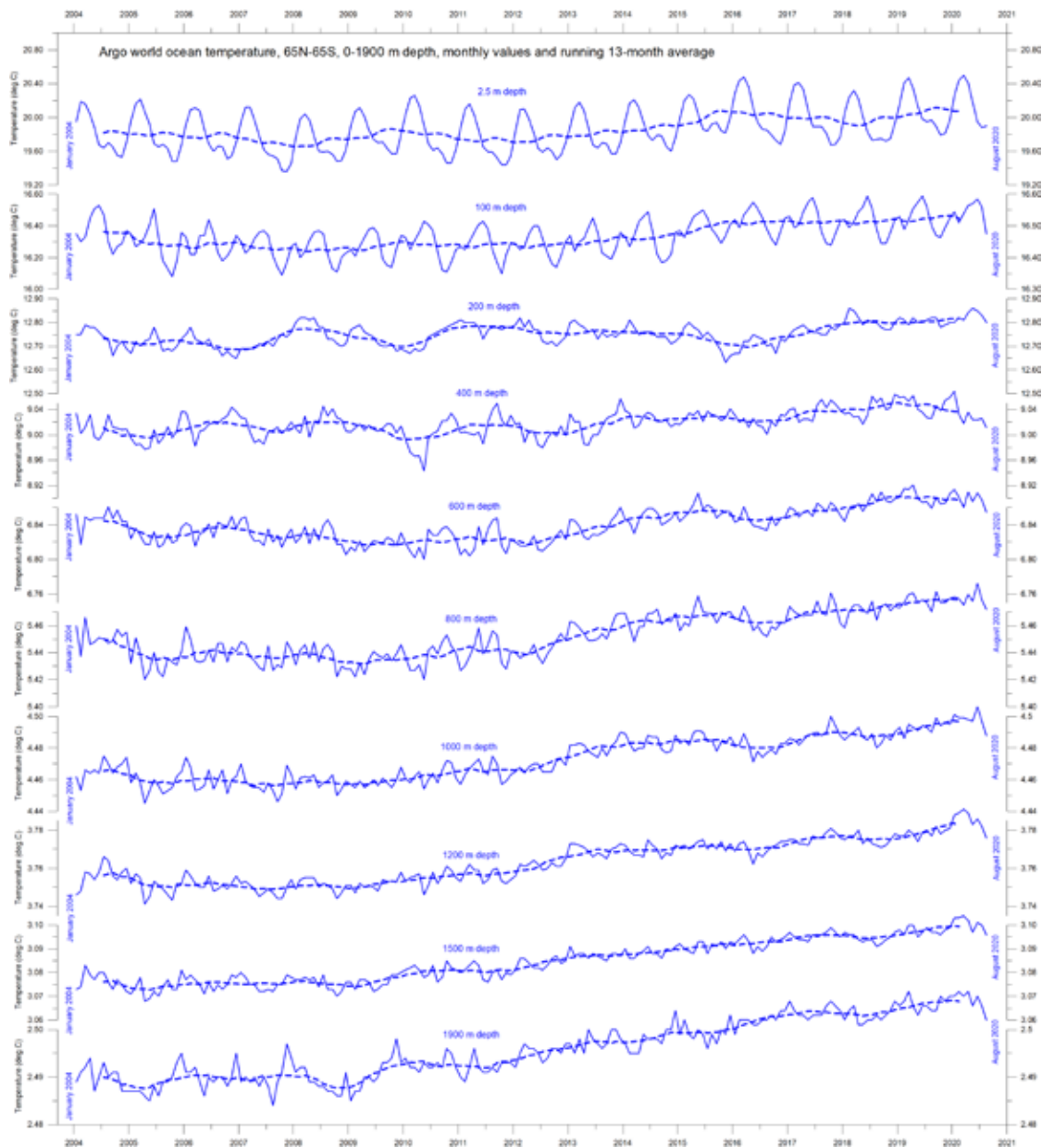


Figure 24: Ocean temperatures at different depths

Ocean temperatures January 2004–August 2020 at different depths between 65°N and 65°S, using Argo data. The thin line shows monthly values, and the dotted line shows the running 13-month average. Source: Global Marine Argo Atlas.

playing out at or near the ocean surface, but also by processes operating at greater depths than 1900 m. As a result, part of the current ocean warming appears to be due to circulation changes taking place at depths below 1900 m, and therefore not directly related to processes operating at or near the surface.

This development is also seen in Figure 25, which shows net changes of global ocean temperatures at different depths, calculated as the net difference between two 12-month averages: for January–December 2004 and September 2019–August 2020. The largest net changes are seen to have occurred in the uppermost 200 m of the water column. However, such average values, although important, also hide many interesting regional details. These are considered in the next section.

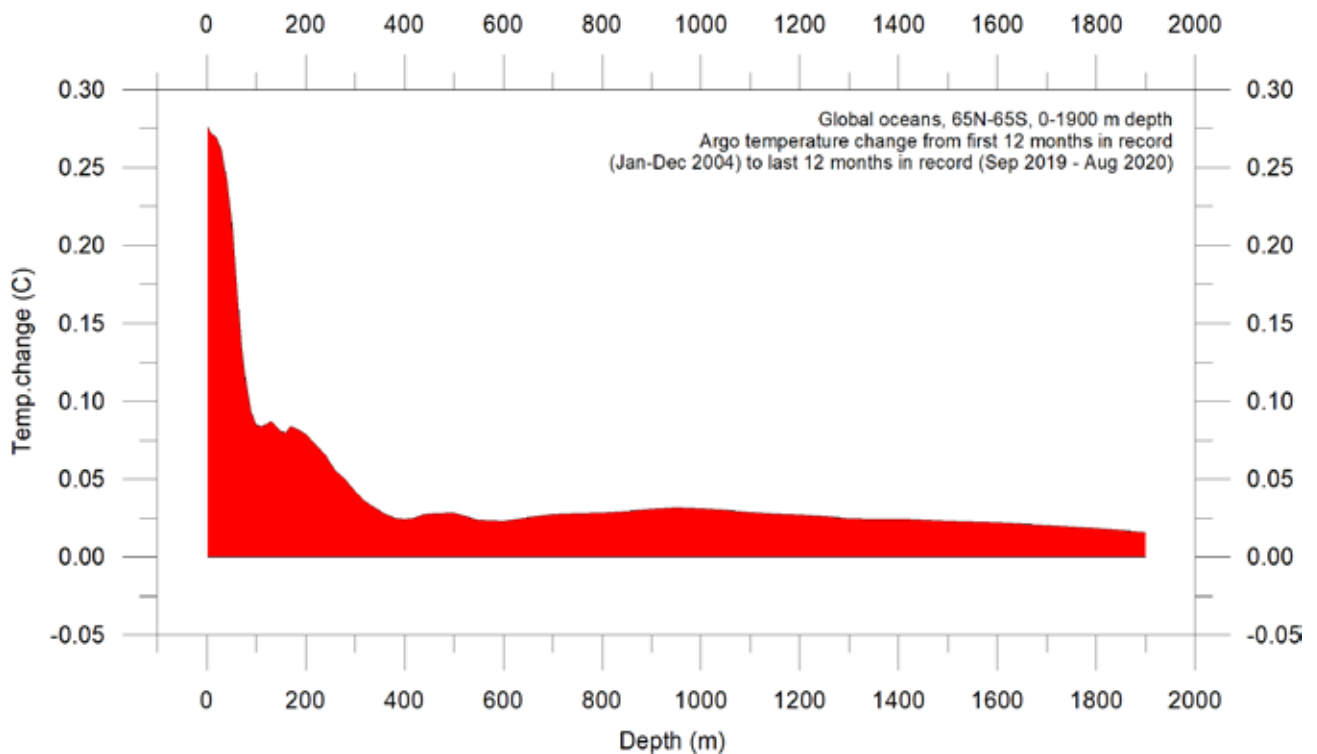


Figure 25: Temperature changes 0–1900 m

Global ocean net temperature change since 2004 from surface to 1900 m depth, using Argo-data. Source: Global Marine Argo Atlas.

By region and depth

Figure 26 shows variation of oceanic temperature net changes between the same two 12-month periods as in the last section, for various depths, and for three different latitudinal bands, representing the Arctic Oceans (55–65°N), Equatorial Oceans (30N–30°S), and Antarctic Oceans (55–65°S), respectively. The global net surface warming shown in Figure 25 can be seen to affect the Equatorial and Antarctic Oceans, but not the Arctic Oceans. In fact, net cooling is pronounced down to 1400 m depth for the northern oceans. However, a major part of Earth’s land area is in the Northern Hemisphere, so the surface area (and volume) of ‘Arctic’ oceans is much smaller than the ‘Antarctic’

oceans, which are in turn smaller than the ‘Equatorial’ oceans. In fact, half of the planet’s surface area (land and ocean) is located between 30°N and 30°S.

Nevertheless, the contrast in net temperature changes for the different latitudinal bands is instructive. For the two polar oceans, the Argo data appears to suggest the existence of a bi-polar seesaw, as described by Chylek et al. (2010). It is no less interesting that the near-surface ocean temperature in the two polar oceans contrasts with the overall development of sea ice in the two polar regions (see later in this report).

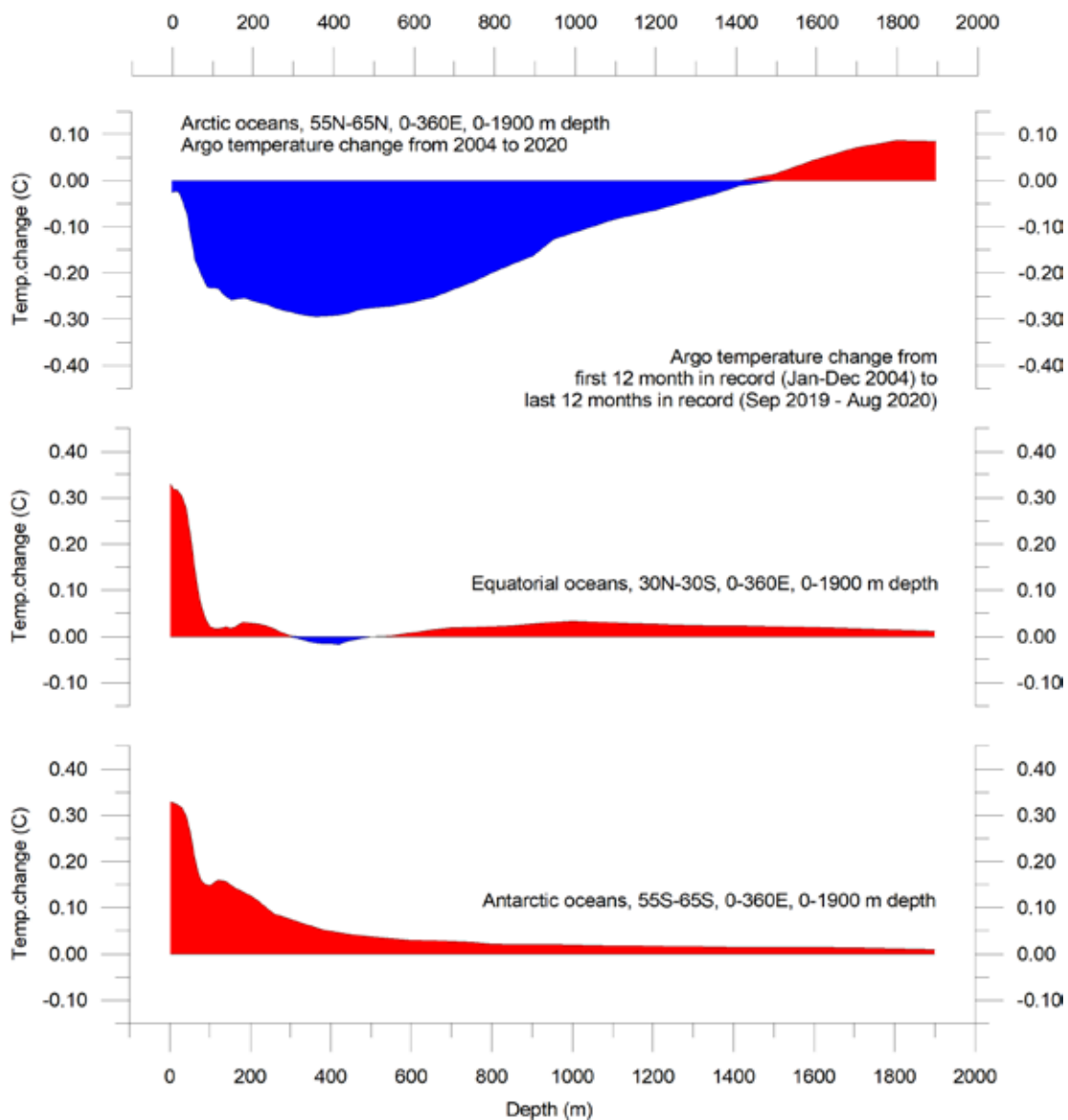


Figure 26: Temperature changes 0–1900 m

Global ocean net temperature change since 2004 from surface to 1900m depth. Source: Global Marine Argo Atlas.

Ocean temperature net change 2004–2020 in selected sectors

Figure 28a shows net temperature changes during 2004–2019 along 20°W, representing the Atlantic Ocean. To prepare the diagram, 12-month average ocean temperatures for 2019 were compared to annual average temperatures for 2004, representing the initial 12 months in the Argo-record. However, the Argo data runs to August 2020, and so, to give an insight into the most recent changes, the 12-month net change from September 2019 to August 2020 is shown in the lower diagram (Figure 28b). Warm colours indicate net warming and blue colours indicate cooling. Due to the spherical form of Earth, high latitudes represent smaller ocean volumes than lower ones near the Equator. With this reservation in mind, the data along the Atlantic transect nevertheless reveal several interesting features.

The most prominent feature in the 2004–2019 profile is a marked net cooling at the surface north of the Equator, especially north of

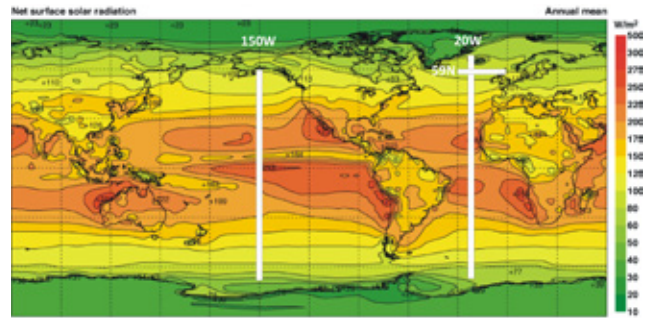


Figure 27: Location of the three profiles

Average annual mean net surface solar radiation (W/m^2), and the location of three profiles discussed below.

45°N. Deeper layers, down to 1500 m depth, are involved. At and south of the Equator, net warming dominates at the surface, but there is net cooling at 50–300 m depth. The maximum net warming is seen between 5°N and 25°S, and affects shallow waters, down to about 50 m. Warming is also seen at latitudes between 10°S and 45°S, between 200 and 1200 m depth.

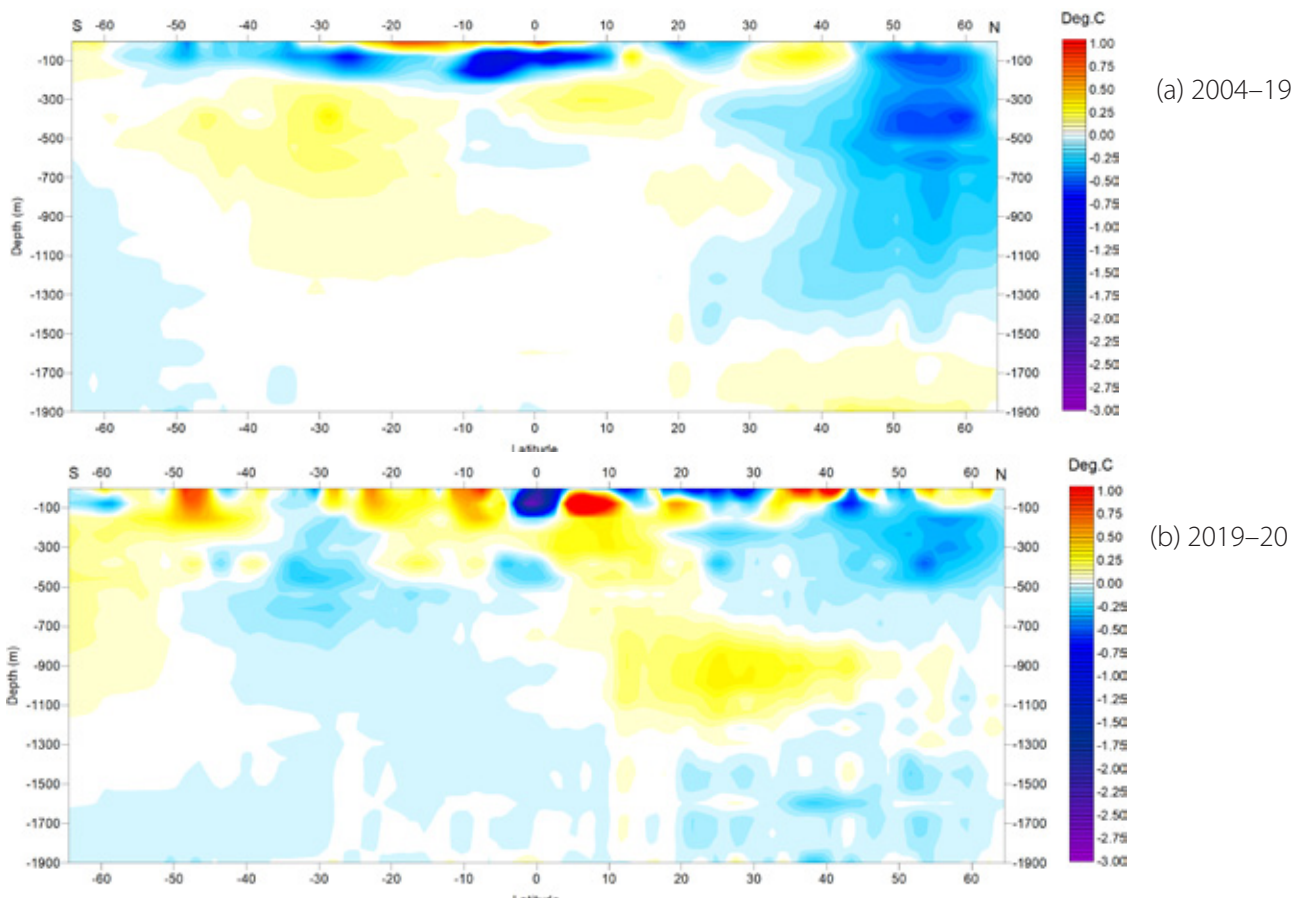


Figure 28: Temperature change along Atlantic profile, 0–1900 m

(a) 2004–2020 and (b) Sept 19–Aug 20. See Figure 27 for geographical location of transect. Data source: Global Marine Argo Atlas.

The temperature development over the last 12 months of the record (Figure 28b) shows a more complicated pattern, especially near the surface. However, the South Atlantic warming at depth appears to be weakening, while the North Atlantic cooling appears to have continued, with the exception of depths between 800 and 1100 m.

Of particular interest are the temperature dynamics displayed within a 59°N transect across the North Atlantic Current, just south of the Faroe Islands, as this area is important for weather and climate in much of Europe. Figure 29 shows a time series at 59°N, from 30°W to 0°W, and from the surface to 800 m depth. This essentially represents a section across the water masses affected by the North Atlantic Current.

Ocean temperatures higher than 9°C are indicated by red colours.

This time series, although still relatively short, display noteworthy dynamics. The prominence of warm water (above 9°C) apparently peaked in early 2006, after which temperatures gradually reduced until 2016. Since then, a partial temperature recovery has taken place. The observed change, from peak to trough, playing out over approximately 11 years, might suggest a 22-year temperature cycle, but we will have to wait until the Argo series is longer before drawing conclusions.

Figure 30 shows the same time series data (59°N, 330–0°W, 0–800 m depth, 2004–2020) as a graph of depth-integrated average ocean temperature.

Figure 29: Temperature change along North Atlantic Current profile, 0–800 m

See Figure 28 for geographical location of transect. Data source: Global Marine Argo Atlas.

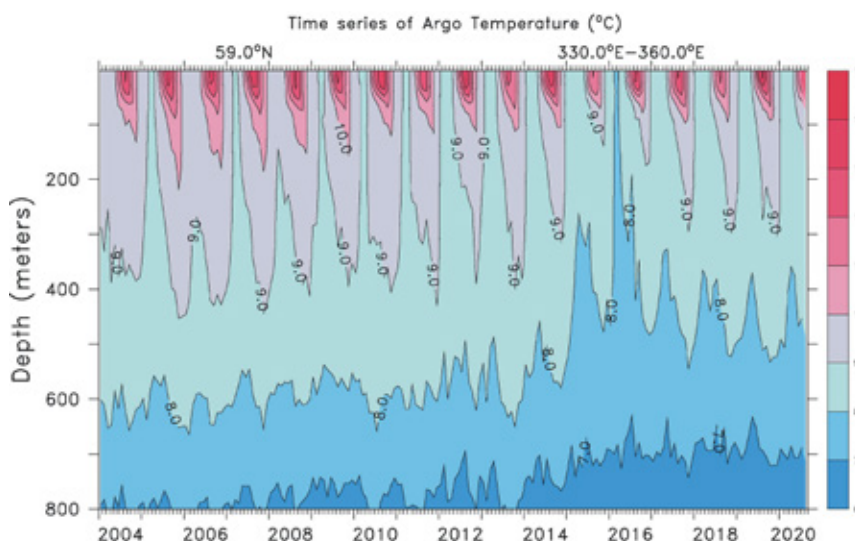


Figure 30: Depth-integrated temperature for the North Atlantic Current profile

See Figure 28 for geographical location of transect. Data source: Global Marine Argo Atlas.

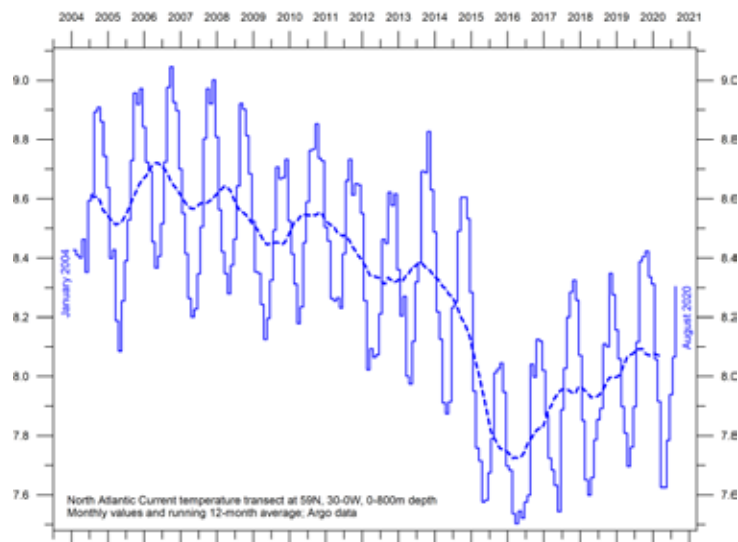


Figure 31 is analogous to Figure 28, but for a transect along 150°W, thus representing the Pacific Ocean (the observations about the volumes represented at high and low latitudes still apply).

Figure 31a represents the changes for 2004–2019, and reveals a slight net cooling affecting nearly all depths down to 1900 m south of 55°S. This contrasts with an overall net warming down to 1000 m north of 55°S. Net warming has been especially prominent between 40°N and 60°N, down to 200 m depth. In contrast, net cooling characterises depths between 100 and 500 m between 5°S and 30°N, and between 20°S and 30°S.

During the last 12 months in the Argo record (Figure 31b) cooling is seen to dominate all

depths between 45°S and 30°N. At least part of this recent temperature development can probably be related to the onset of La Niña towards the end of 2020 (Figure 22).

Neither the Atlantic nor the Pacific longitudinal diagrams reveal the extent to which the net changes displayed are caused by ocean dynamics operating east and west of the two profiles considered. For that reason, they should not be overinterpreted. They do, however, suggest an interesting contrast, with the Pacific mainly warming, especially north of Equator, and cooling in the south, while the opposite is true of the Atlantic: cooling in the north and warming in the south.

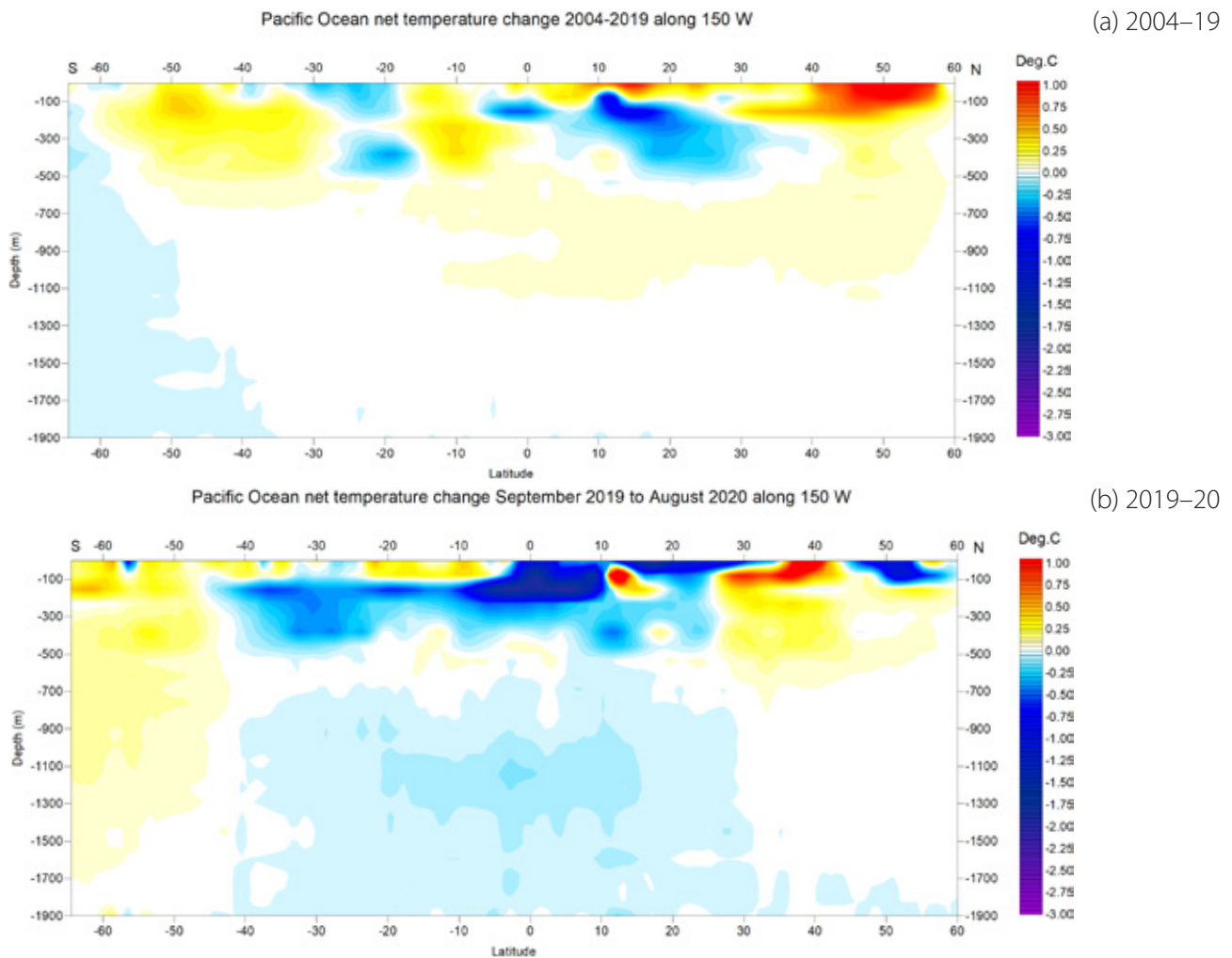


Figure 31: Temperature change along Pacific profile, 0–1900 m

(a) 2004–2020 and (b) Sept 19–Aug 20. See Figure 28 for geographical location of transect. Data source: Global Marine Argo Atlas.

4. Oceanic oscillations

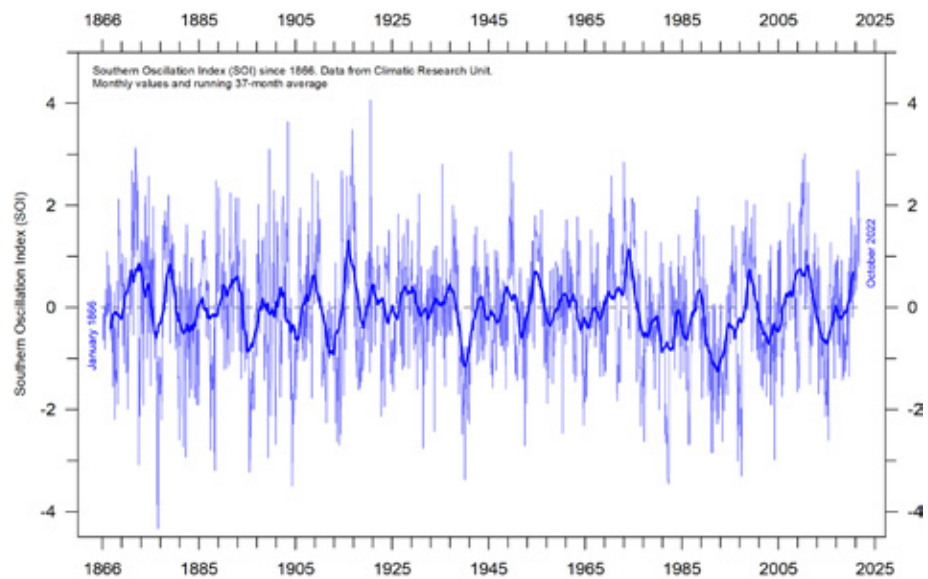
Southern Oscillation Index

The Southern Oscillation can be considered the atmospheric component of El Niño/La Niña episodes. Sustained negative values of the SOI (Figure 32) often indicate El Niño episodes. Such negative values are usually accompanied by persistent warming of the central and eastern tropical Pacific Ocean, a decrease in the strength of the Pacific Trade Winds, and a reduction in rainfall over eastern and northern Australia.

Positive values of the SOI are usually associated with stronger Pacific trade winds and higher sea-surface temperatures to the north of Australia, indicating La Niña episodes. Waters in the central and eastern tropical Pacific Ocean become cooler at such times. Eastern and northern Australia usually receive increased precipitation during such periods.

Figure 32: Annual SOI anomaly since 1866

The thin line represents annual values, while the thick line is the simple running 5-year average. Source: Climatic Research Unit, University of East Anglia.



Pacific Decadal Oscillation

The PDO (Figure 33) is a long-lived El Niño-like pattern of Pacific climate variability, with data extending back to January 1900. Its causes are not currently known, but even in the absence of a theoretical understanding, taking into account its variability improves season-to-season and year-to-year climate forecasts for North America because of its strong tendency for multi-season and multi-year persistence. The PDO also appears to be roughly in phase with global temperature changes. Thus it is important from a societal-impact perspective, because it shows that 'normal' climate conditions can vary over periods comparable to the length of a human lifetime.

The PDO nicely illustrates how global temperatures are tied to sea-surface temperatures in the Pacific Ocean, the largest ocean on Earth. When sea-surface temperatures are relatively low (negative phase PDO), as they were from 1945 to 1977, global air temperature decreases. When sea-surface temperatures are high (positive phase PDO), as they were from 1977 to 1998, global surface air temperature increases (Figures 12–14).

A Fourier frequency analysis (not shown here) shows the PDO record to be influenced by a 5.7-year cycle, and possibly also by a longer cycle of about 53-years.

Atlantic Multidecadal Oscillation

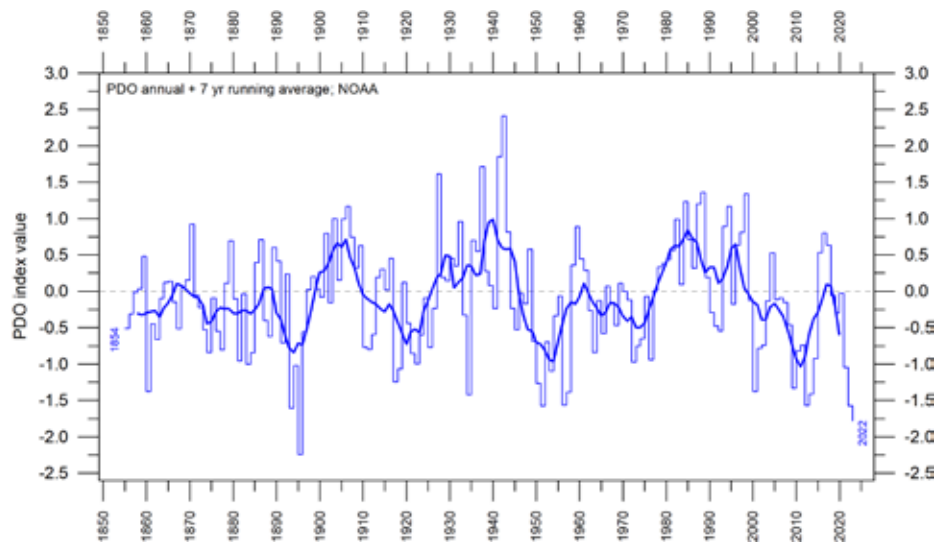
The Atlantic Multidecadal Oscillation (AMO; Figure 34) is a mode of variability occurring in the North Atlantic Ocean sea-surface temperature

field. The AMO is essentially an index of North Atlantic sea-surface temperatures (SST).

The AMO index appears to be correlated to

Figure 33: Annual values of the Pacific Decadal Oscillation (PDO) according to the Physical Sciences Laboratory, NOAA.

The thin line shows the annual PDO values, and the thick line is the simple running 7-year average. Source: PDO values from NOAA Physical Sciences Laboratory: ERSST V5 <https://psl.noaa.gov/pdo/>



air temperatures and rainfall over much of the Northern Hemisphere. The association appears to be high for northeastern Brazil, African Sahel rainfall and North American and European summer climate. The AMO index also appears to be associated with changes in the frequency of North American droughts and is reflected in the frequency of severe Atlantic hurricanes.

As one example, the AMO index may be related to the past occurrence of major droughts in the US Midwest and the Southwest. When the AMO is high, these droughts tend to be more frequent or prolonged, and vice-versa for

low values. Two of the most severe droughts of the 20th century in the US – in the 1950s and 1930s’ ‘Dust Bowl’ – occurred during a time of peak AMO values, which lasted from 1925 to 1965. On the other hand, Florida and the Pacific Northwest tend to experience an opposite effect, high AMO in these areas being associated with relatively high precipitation.

A Fourier-analysis (not shown here) shows the AMO record exhibits a cycle of around 67-years’ duration, and to a lesser degree by another of 3.5-years.

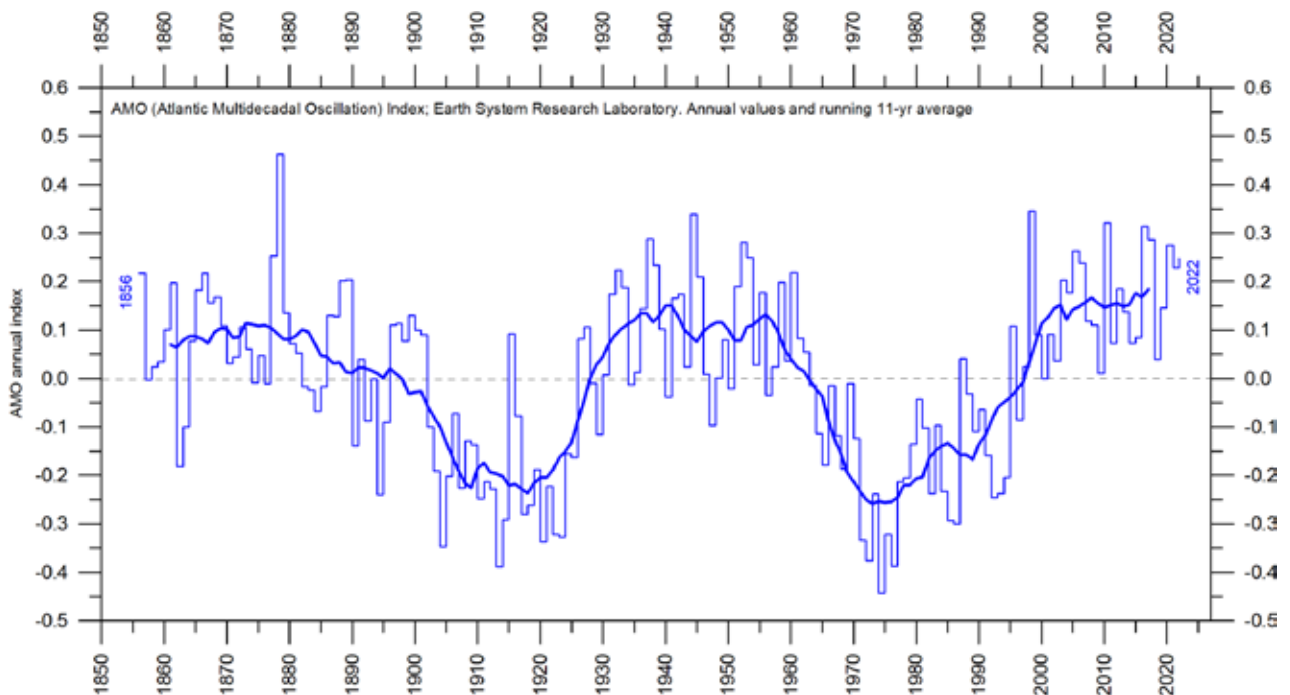


Figure 34: The Atlantic Multidecadal Oscillation

Annual Atlantic Multidecadal Oscillation (AMO) detrended and unsmoothed index values since 1856. The thin blue line shows annual values, and the thick line is the simple running 11-year average. Data source: Earth System Research Laboratory, NOAA, USA.

5. Sea-level

In general

Global, regional, and local sea levels always change. During the last glacial maximum, about 20–25,000 years ago, global sea levels were around 120 m lower than modern ones. Since the end of the so-called Little Ice Age, about 100–150 years ago, global sea levels have on average increased 1–2 mm/year, according to tide gauge data.

Global (or eustatic) sea-level change is measured relative to an idealised reference level, the geoid, which is a mathematical model of planet Earth's surface (Carter et al. 2014). Global sea-level is a function of the volume of the ocean basins and the volume of water they contain. Changes in global sea-level are caused by – but not limited to – four main mechanisms:

- Changes in local and regional air pressure and wind, and tidal changes introduced by the Moon.
- Changes in ocean basin volume by tectonic (geological) forces.
- Changes in ocean water density caused by variations in currents, water temperature and salinity.
- Changes in the volume of water caused by changes in the mass balance of terrestrial glaciers.

There are also some other mechanisms influencing sea level: storage of ground water, storage in lakes and rivers, evaporation, and so on.

Ocean basin volume changes occur too slowly to be significant over human lifetimes and it is therefore the mechanisms 3 and 4 that drive contemporary concerns about sea-level rise.

Higher temperature in itself is only a minor factor contributing to global sea-level rise, because seawater has a relatively small coefficient of expansion and because, over the timescales of interest, any warming is largely confined to the upper few hundred metres of the ocean surface.

The growth or decay of sea ice has no influence on sea level. However, the melting of land-

based ice – including both mountain glaciers and the ice sheets of Greenland and Antarctica – is more significant. As already noted, sea-levels were about 120 m lower during the last glacial maximum. During the most recent interglacial, about 120,000 years ago, global temperatures and thus sea levels were higher than today, because significant parts of the Greenland ice sheet melted.

On a regional and local scale, however, air pressure, wind and the geoid must also be considered. As an example, changes in the volume of the Greenland ice sheet will affect the geoid in adjacent regions; if the mass diminishes, the geoid surface will be displaced towards the centre of the Earth, and sea levels in the region will drop. This will happen even though the overall volume of water in the global oceans increases as glacier ice is lost.

In northern Europe, another factor must also be considered when estimating the future sea level. Norway, Sweden, Finland, and Denmark were all totally or partly covered by the European ice sheet 20–25,000 years ago. Even today, the effect of this ice load is seen in the ongoing isostatic land rise in the area, of several millimetres per year. At many sites this more than compensates for the slow global sea-level rise, so a net sea-level fall in relation to the land is recorded.

The relative movement of sea level in relation to land is what matters for coastal planning, and this is termed the 'relative sea level change'. This is what is recorded by tide gauges.

From satellite altimetry

Satellite altimetry is a relatively new type of measurement, providing unique and valuable insights into changes in the detailed surface topography of the oceans, with nearly global coverage. However, it is probably not a precise tool for estimating absolute changes in global sea level due to interpretation issues surrounding the original satellite data.

The most important is the Glacial Isostatic Adjustment (GIA), a correction for the large-scale, long-term mass transfer from the oceans to the land that results from the waxing and waning of the large Quaternary ice sheets in North America and northern Europe. This enormous mass transfer causes changes in surface

load, resulting in viscoelastic mantle flow and elastic effects in the upper crust. It is hard to correct the satellite data for this effect, since no single technique or observational network can give enough information. Researchers therefore have to resort to modelling, and the answer they get depends upon the type of deglaciation model (for the last glaciation) and upon the type of crust-mantle model that is assumed. Because of this (and other factors), estimates of global sea-level change based on satellite altimetry vary somewhat.

In Figure 35, the global sea-level rise estimate is about 3.4 mm/year (since 1992), with the estimated GIA effect removed. Linear trends

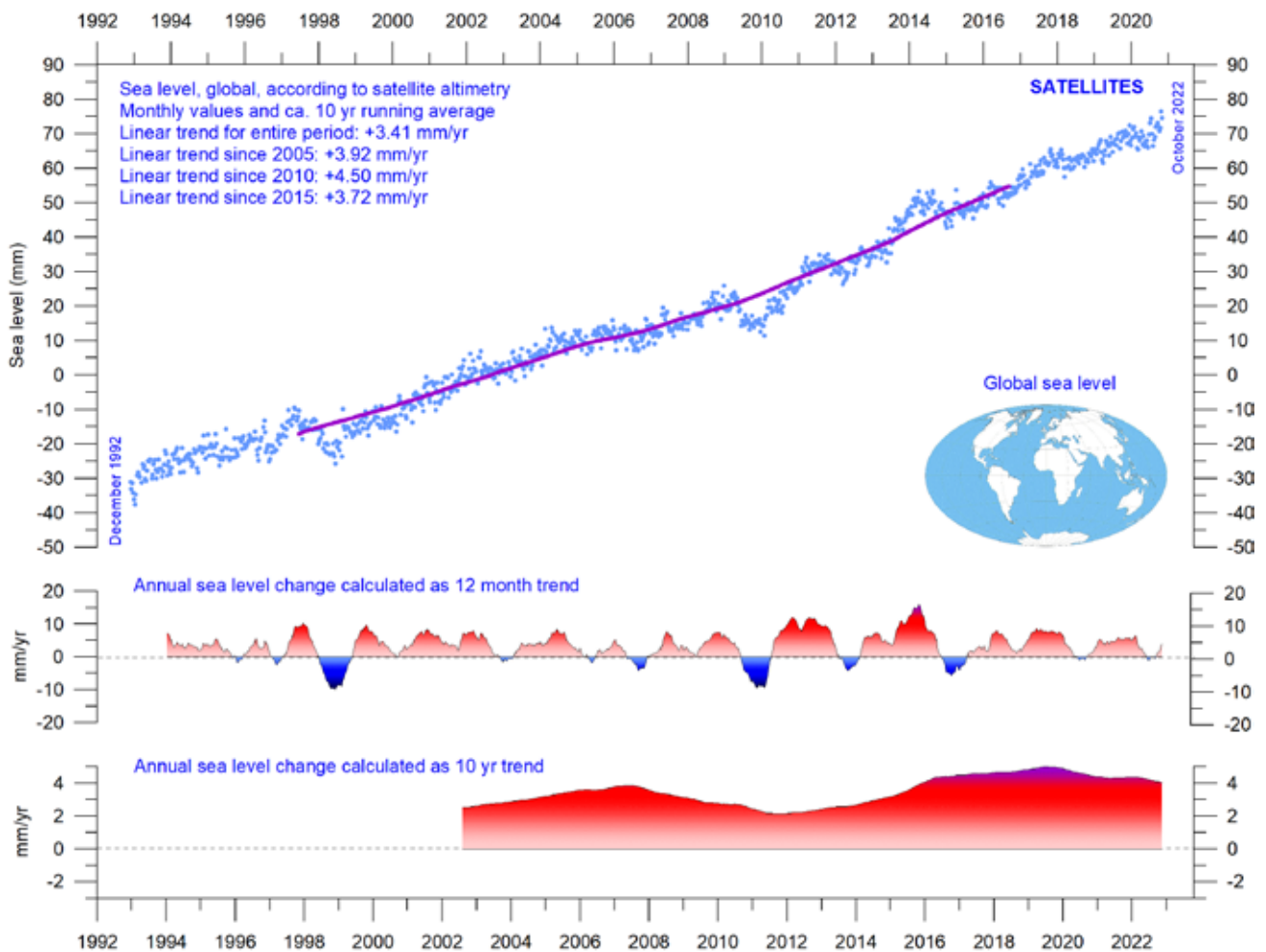


Figure 35: Global sea level change since December 1992

The two lower panels show the annual sea level change, calculated for 1- and 10-year time windows, respectively. These values are plotted at the end of the interval considered. Source: Colorado Center for Astrodynamics Research at University of Colorado at Boulder. The blue dots are the individual observations (with calculated GIA effect removed), and the purple line represents the running 121-month (ca. 10-year) average.

calculated since 2005, 2010 and 2015 do not suggest any recent acceleration, and the lower

panel in Figure 35 instead suggests that a sea-level rise peak was reached in around 2019.

From tide-gauges

Tide-gauges are located at coastal sites and record the net movement of the local ocean surface in relation to land. These measurements (see, for example, Figure 36) are key information for local coastal planning, and are directly applicable for planning coastal installations, in contrast to satellite altimetry.

At any specific coastal site, the measured net movement of the local coastal sea-level comprises two local components:

- the vertical change of the ocean surface
- the vertical change of the land surface.

For example, a tide-gauge may record an apparent sea-level increase of 3 mm/year. If geodetic measurements show the land to be sinking by 2 mm/year, the real sea-level rise is only 1 mm/year (3 minus 2 mm/year). In a global sea-level change context, the value of 1 mm/year is rele-

vant, but in a local coastal planning context the 3 mm/year tide-gauge value is the one that is useful for local planning authorities.

To construct a time series of sea-level measurements at each tide-gauge, the monthly and annual means must be reduced to a common datum. This reduction is performed by the Permanent Service for Mean Sea Level (PSMSL), making use of data provided by the national authorities. The Revised Local Reference (RLR) datum at each station is defined to be approximately 7000 mm below mean sea level, with this arbitrary choice made many years ago to avoid negative numbers in the resulting RLR monthly and annual mean values.

Few places on Earth are completely stable, and most tide-gauges are located at sites exposed to tectonic uplift or sinking (the vertical change of the land surface). This widespread

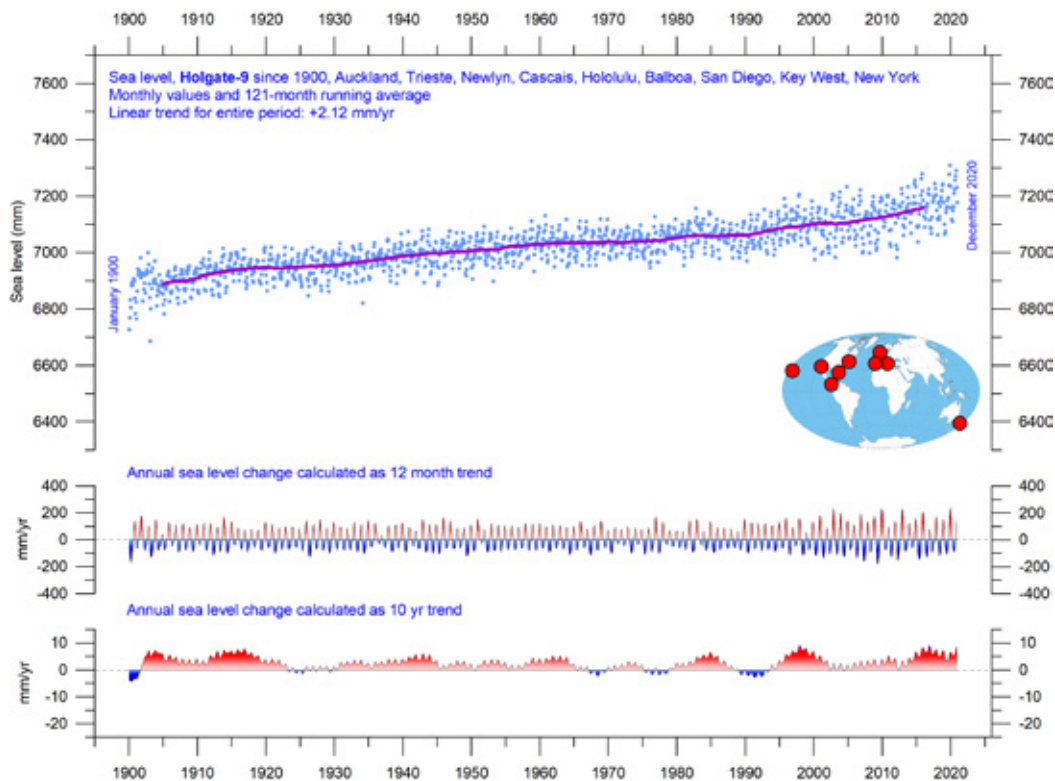


Figure 36: Holgate-9 monthly tide gauge data from PSMSL Data Explorer

The Holgate-9 are a series of tide gauges located in geologically stable sites. The two lower panels show the annual sea level change, calculated for 1- and 10-year time windows, respectively. These values are plotted at the end of the interval considered. Source: Colorado Center for Astrodynamics Research at University of Colorado at Boulder. The blue dots are the individual observations, and the purple line represents the running 121-month (ca. 10-year) average.

vertical instability has several causes and affects the interpretation of data from the individual tide-gauges. Much effort is therefore put into correcting for local tectonic movements.

As a result, data from tide-gauges located at tectonic stable sites is of special interest. One example of a long, continuous record from such a site is from Korsør, Denmark (Figure 37). This record indicates a stable sea-level rise of about 0.83 mm per year since 1897, without any sign of recent acceleration.

Data from tide-gauges all over the world suggest an average global sea-level rise of about 1–2 mm/year, while the satellite-derived record (Figure 35) suggests a rise of about 3.4 mm/year, or more. The noticeable difference (just about 1:2) between the two data sets is remarkable but has no generally accepted explanation. It is, however, known that satellite observations face complications in areas near the coast. Vignudelli et al. (2019) provide an updated overview of the current limitations of classical satellite altimetry in coastal regions.

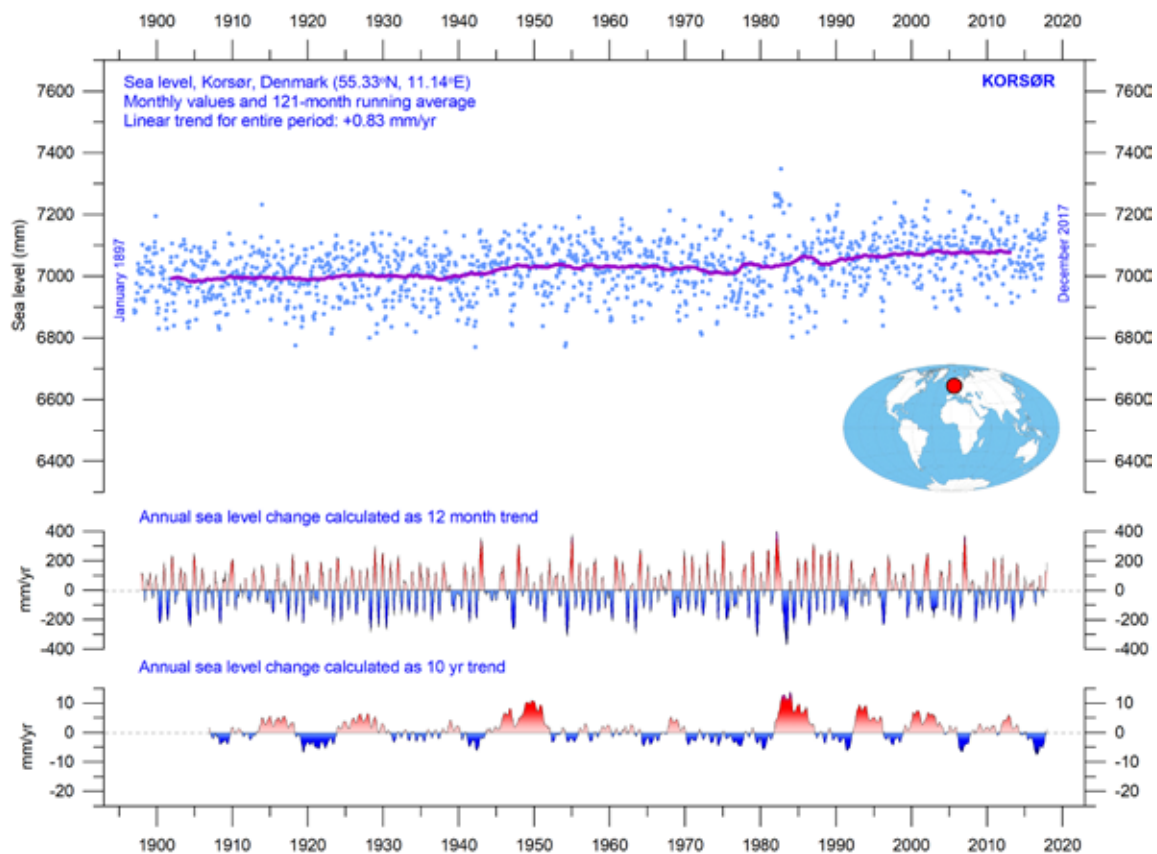


Figure 37: Korsør (Denmark) monthly tide gauge data

From PSMSL Data Explorer. The blue dots are the individual monthly observations, and the purple line represents the running 121-month (ca. 10-year) average. The two lower panels show the annual sea level change, calculated for 1- and 10-year time windows, respectively. These values are plotted at the end of the interval considered.

Modelled for the future

The issue of sea-level change, and in particular the identification of a hypothetical human contribution to that change, is a complex topic. Given the scientific and political controversy that surrounds the matter, the great public interest in this area is entirely understandable.

A recent IPCC publication, the 6th Assessment Report from Working Group I, was released on August 9th, 2021. Modelled data for global and regional sea-level projections 2020–2150 are available from the IPCC AR6 Sea Level Projection Tool (see link at the end of this report). The IPCC models future development of several factors, such as glacier mass change, vertical land movement, water temperature and storage. Modelled sea-level projections for different emissions scenarios are calculated relative to a baseline defined by observations for 1995–2014.

It is enlightening to compare the modelled data with observed sea-level data. Figure 38 shows this for one location, namely Oslo. Norway was totally covered by the European Ice Sheet 20–25,000 years ago, with more than 2 km of ice over the city at the maximum glaciation. Today, the effect of this ice load is clearly demonstrated by the fact that southern Norway experiences an ongoing isostatic land rise of several millimetres per year. At many sites affected by the last (Weichselian/Wisconsin) glaciation, this ongoing isostatic movement more than compensates for the slow global sea-level rise, so a net sea-level decrease in relation to land is recorded.

As Oslo was covered by thick ice during the last glaciation, it is affected by a marked isostatic land rise today. If the observed sea-level change rate at Oslo continues (based on about 110 years of observations), by 2100, the relative sea-level (in relation to land) will have dropped by about 27 cm relative to 2020 (Figure 38). However, according to the IPCC, it will have increased about 17.5 cm. It projects a rather sudden increase in 2020, which contrasts with the stable sea-level decline of about -3.39 mm/yr recorded since 1914. Observed (measured) and modelled data now have an overlap of 3 years (Figure 38).

The overlap period is still short, but it seems to suggest an unbroken sea-level decrease at Oslo since 2020, in contrast to the model projection (blue line in Figure 38).

A few reflections might be appropriate at this point. The step change in relative sea-level dynamics for Oslo (and many other coastal sites) in 2020 appears rather implausible and suggests that the modelled data is not describing the real-world dynamics adequately. This is remarkable, as the modelled sea-level projections for different SSP scenarios are calculated relative to a baseline defined by observations 1995–2014, for each station. The modelers must therefore have seen the observed data.

According to the 6th Assessment Report, human activities are estimated to have caused approximately 1.0°C of global warming above pre-industrial levels, with a likely range of 0.8 – 1.2°C (Summary for Policymakers, A.1.3). It is therefore particularly surprising that the modelled effect of this change should first affect sea levels in the shape of a step change in 2020. Had the modelers instead calibrated their sea-level data from an earlier date, say 1950, which would have been completely possible, the contrast between observed and modelled data would immediately have become apparent.

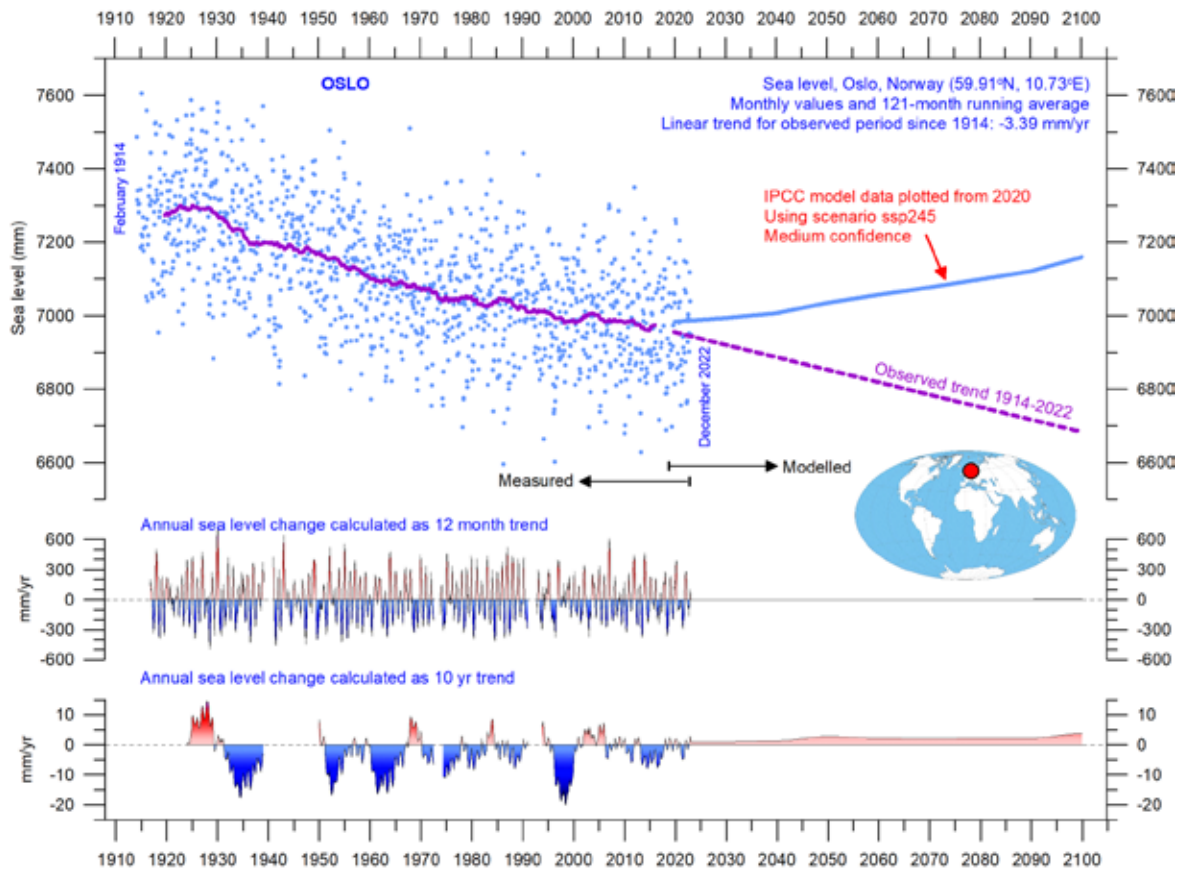


Figure 38: Observed and modelled sea level for Oslo.

The blue dots are the individual monthly tide gauge observations (PSMSL Data Explorer) 1914–2019, and the purple line represents the running 121-month (ca. 10-year) average. The modelled data for the future is shown by a solid blue line 2020–2100, using the moderate SSP2–4.5 scenario (IPCC 2020). The two lower panels show the annual sea-level change, calculated for 1- and 10-year time windows, respectively. These values are plotted at the end of the interval considered.

6. Snow and ice

The two 12-month average sea-ice extent graphs in Figure 39 display a contrasting development between the two poles over the period 1979–2020. The Northern Hemisphere sea-ice trend towards smaller extent is clearly displayed by the blue lined, and so is the simultaneous increase in the Southern Hemisphere until 2016. In many respects, this and previous observations presented in this report suggest that the year 2016 may well mark an important shift in the global climate system.

The Antarctic sea-ice extent decreased extraordinarily rapidly during the Southern Hemisphere spring of 2016, much faster than in any previous spring during the satellite era (since 1979). A strong ice retreat occurred in all sectors of the Antarctic, but was greatest in the Weddell and Ross Seas. In these sectors, strong

northerly (warm) surface winds pushed the sea ice back towards the Antarctic continent. The background for the special wind conditions in 2016 has been discussed by various authors (e.g. Turner et al. 2017 and Phys.org 2019), and appears to be a phenomenon related to natural climate variability. The satellite sea-ice record is still short, and does not fully represent natural variations playing out over more than a decade or two.

What can be discerned from the still short record is nevertheless instructive. The two 12-month average graphs in Figure 40 show recurring variations superimposed on the overall trends. This shorter variation is for the Arctic sea ice, which is strongly influenced by a 5.3-year periodic variation, while for the Antarctic a periodic variation of about 4.5 years is important.

Both these variations reached their minima simultaneously in 2016, which at least partly explains the simultaneous minimum in global sea-ice extent.

In coming years, the variations identified above may again induce an increase in sea-ice extent at the poles, with a derived increase in the 12-month average global sea-ice extent as the possible result. In fact, this may already be happening in both the Arctic and the Antarctic

(Figure 39). However, in coming years, minima and maxima for these variations will not occur synchronously because of their different period lengths, and global minima (or maxima) may therefore be less pronounced than in 2016.

Figure 40 illustrates the overall extent and thickness of the Arctic sea-ice from the end of 2021 to the end of 2022. Sea-ice thickness has been increasing along the coasts of Canada and Greenland during 2022.

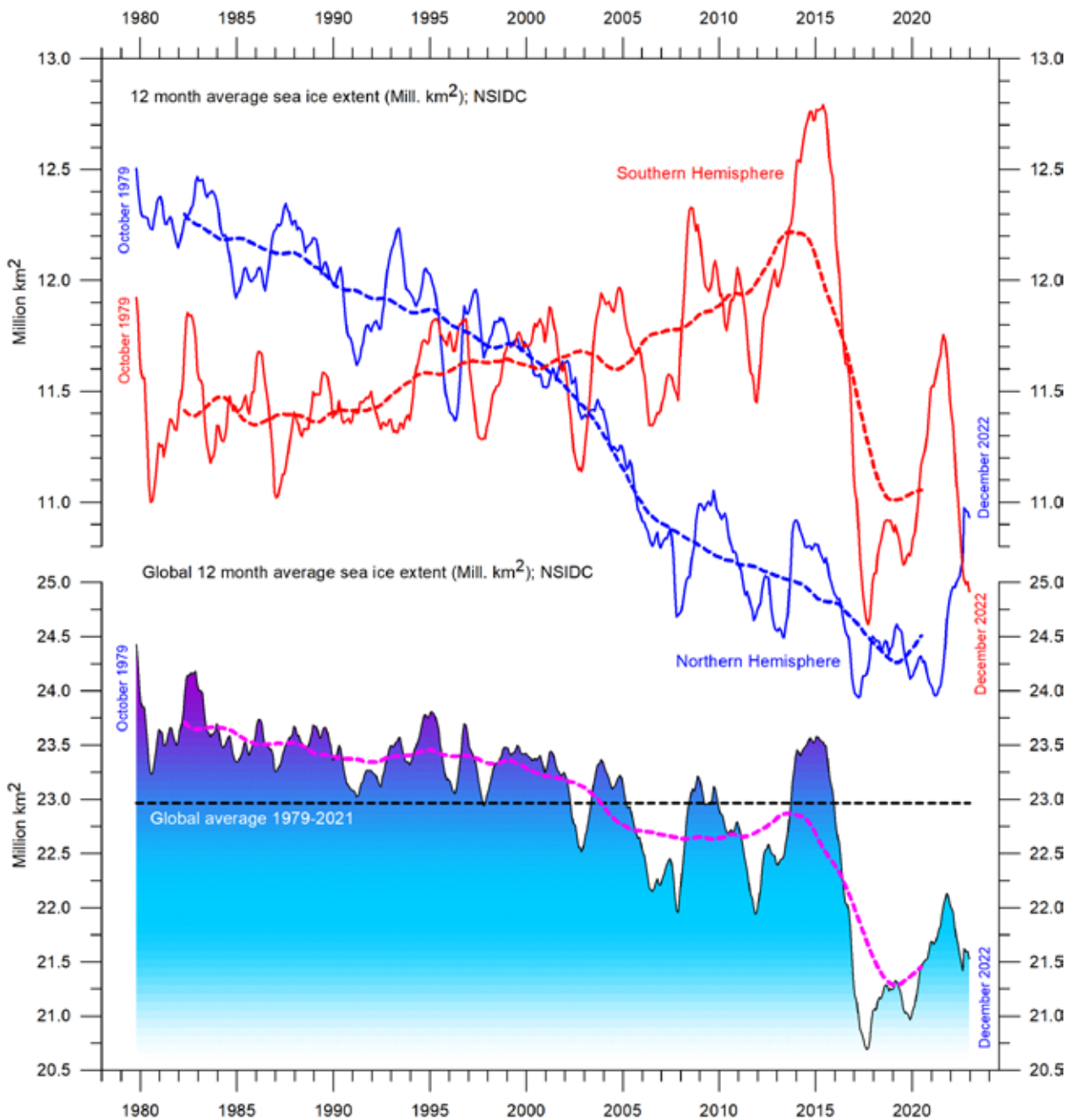


Figure 39: Global and hemispheric sea ice extent since 1979

12-month running means. The October 1979 value represents the monthly average of November 1978–October 1979, the November 1979 value represents the average of December 1978–November 1979, etc. The stippled lines represent a 61-month (ca. 5 years) average. The last month included in the 12-month calculations is shown to the right in the diagram. Data source: National Snow and Ice Data Center (NSIDC).

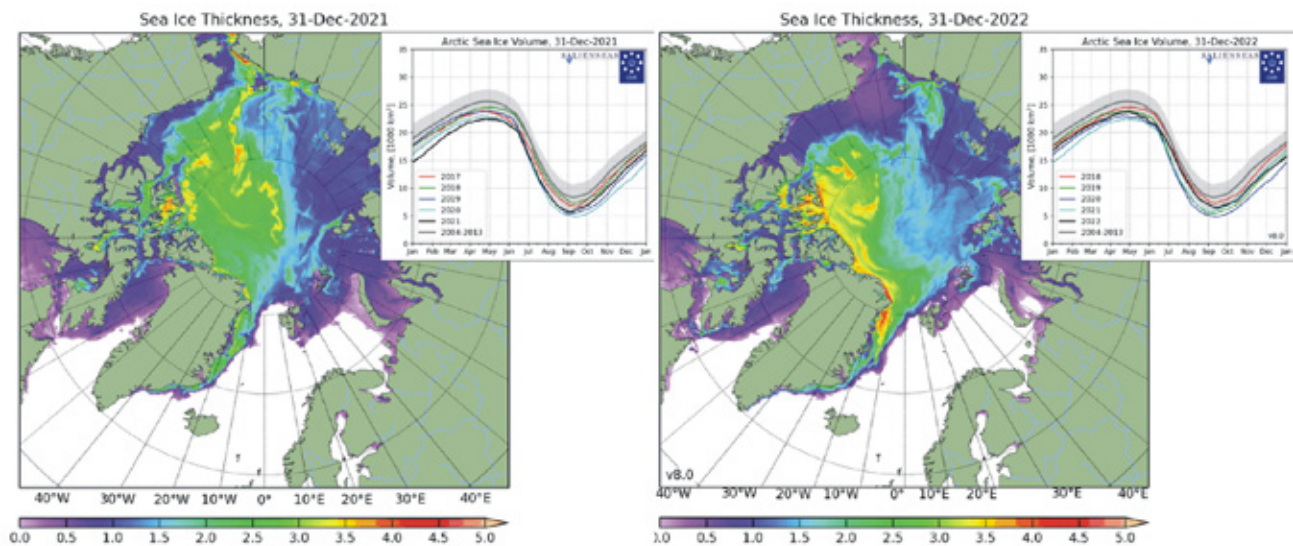


Figure 40: Arctic sea ice 2021 versus 2022

Arctic sea-ice extent and thickness 31 December 2021 (left) and 2022 (right) and the seasonal cycles of the calculated total arctic sea ice volume, according to the Danish Meteorological Institute (DMI). The mean sea ice volume and standard deviation for the period 2004–2013 are shown by grey shading in the insert diagrams.

Northern Hemisphere snow cover

Variations in the global snow cover are mainly the result of changes playing out in the Northern Hemisphere (Figure 41), where all the major land areas are located. The Southern Hemisphere snow cover is essentially controlled by the Antarctic ice sheet, and therefore relatively stable.

Northern Hemisphere snow cover is exposed to large local and regional variations from year to year (Figure 42). However, the overall tendency (since 1972) is towards quasi-stable conditions, as illustrated by Figure 43. During the

Northern Hemisphere summer, the snow cover usually shrinks to about 2,400,000 km² (principally controlled by the size of the Greenland ice sheet), but during the winter it increases to about 50,000,000 km², representing no less than 33% of planet Earth's total land area. Considering seasonal changes (Figure 43), the Northern Hemisphere snow cover has slightly increased during autumn, is stable at mid-winter, and is slightly decreasing in spring. In 2022, the Northern Hemisphere snow cover extent was close to the 1972–2021 average (Figure 44).

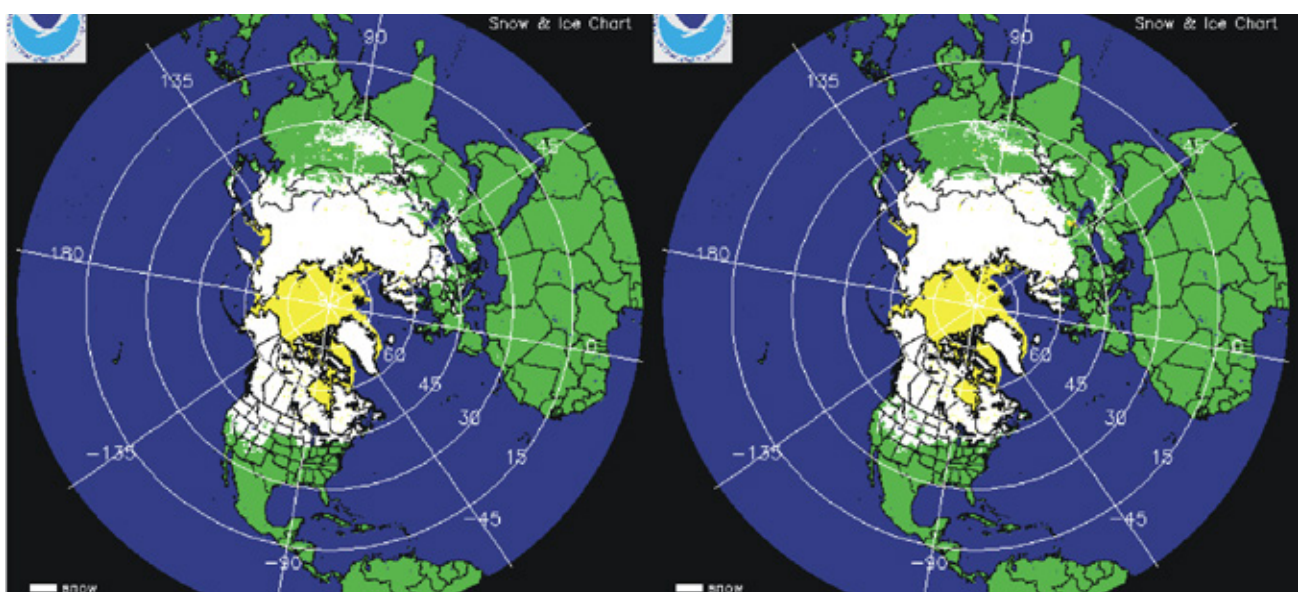


Figure 41: Northern hemisphere snow and sea ice

Snow cover (white) and sea ice (yellow) 31 December 2021 (left) and 2022 (right). Map source: National Ice Center (NIC).

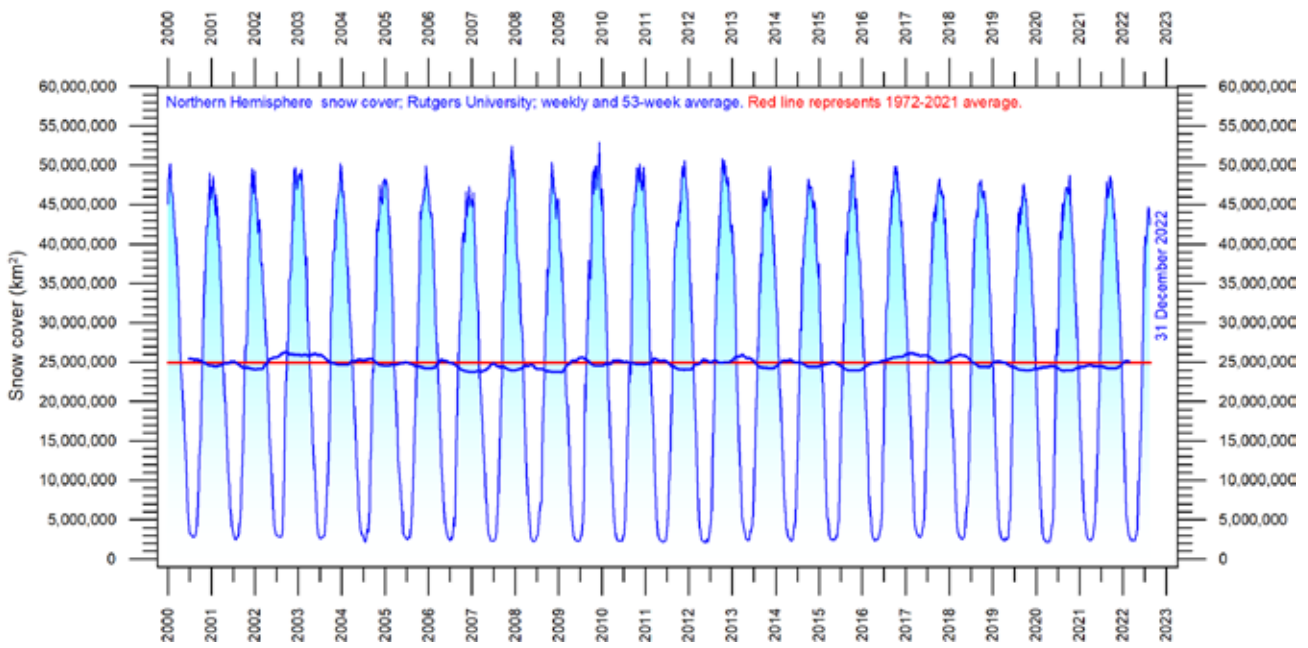


Figure 42: Northern hemisphere weekly snow cover since 2000

Source: Rutgers University Global Snow Laboratory. The thin blue line is the weekly data, and the thick blue line is the running 53-week average (approximately 1 year). The horizontal red line is the 1972–2020 average.

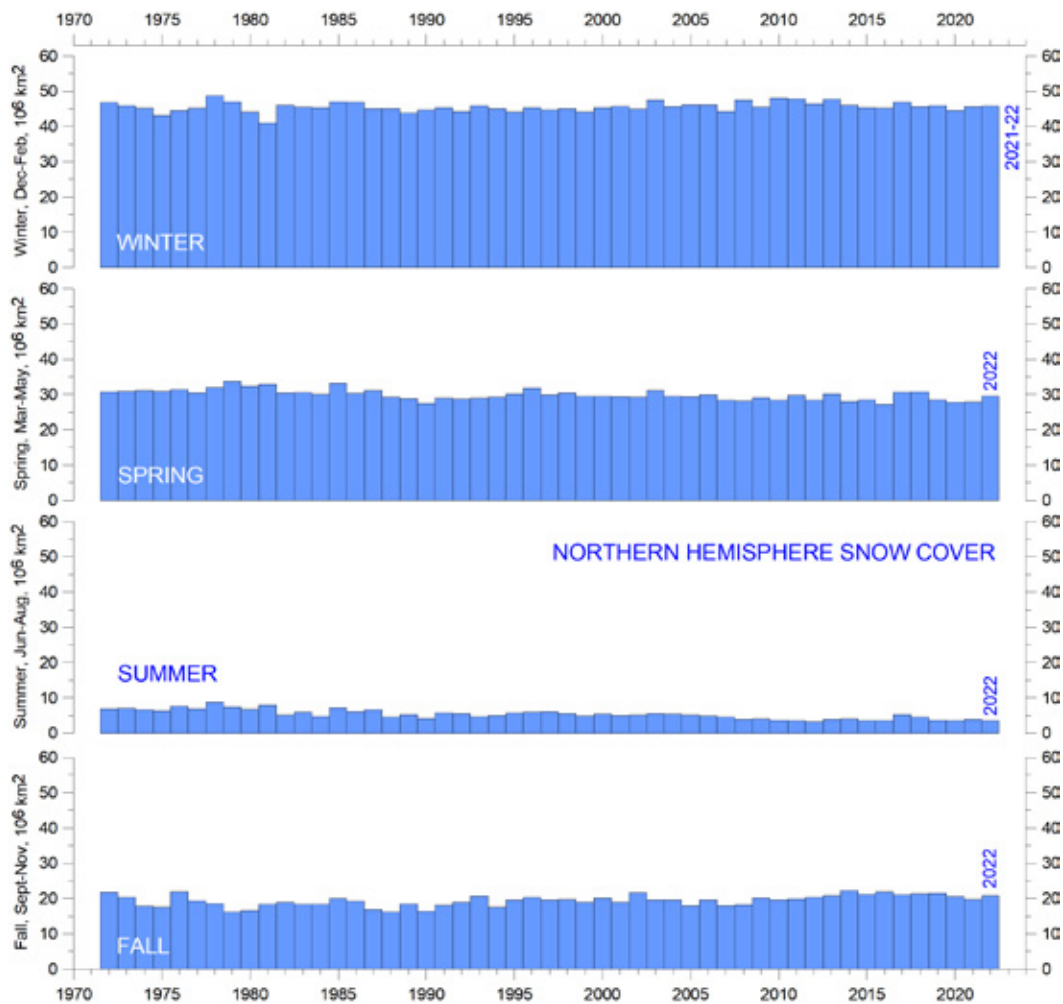


Figure 43: Northern Hemisphere seasonal snow cover since 1972

Source: Rutgers University Global Snow Laboratory.

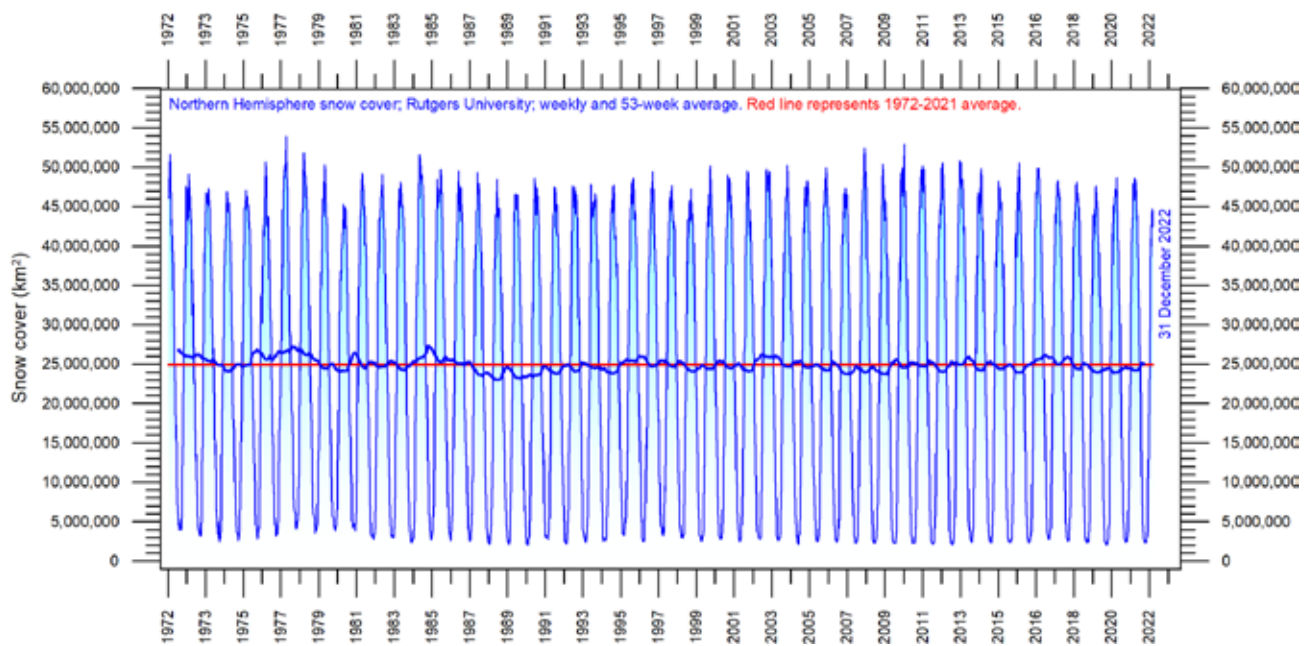


Figure 44: Northern hemisphere weekly snow cover since 1972

Source: Rutgers University Global Snow Laboratory. The thin blue line is the weekly data, and the thick blue line is the running 53-week average (approximately 1 year). The horizontal red line is the 1972–2020 average.

7. Tropical storm and hurricanes

Accumulated cyclone energy

Accumulated cyclone energy (ACE) is a measure used by NOAA to express the activity of individual tropical cyclones and entire tropical cyclone seasons. ACE is calculated as the square of the wind speed every six hours, and is then scaled by a factor of 10,000 for usability, using a unit of 10^4 knots². The ACE of a season is the sum of the ACE for each storm, and therefore encapsulates the number, strength, and duration of all the tropical storms in the season. The ACE data and ongoing cyclone dynamics are detailed in Maue (2011).

The damage potential of a hurricane is proportional to the square or cube of the maximum wind speed, and thus ACE is not only a measure of tropical cyclone activity, but also a measure of the damage potential of an individual cyclone or a season. Existing records (Figure 45) do not suggest any abnormal cyclone activity in recent years.

The global ACE data since 1970 display a variable pattern over time, but without any clear trend, as are the diagrams for the Northern- and Southern Hemisphere (panels in Figure 45). A Fourier analysis (not shown here) indicates a significant oscillation of about 3.6 years' duration, and also suggests a second one, of 11.5-years' period, but the data series is still too short to draw firm conclusions.

The period 1989–1998 was characterised by high values. Other peaks were seen 2004, 2015 and 2018, and the periods 1973–1988, 1999–2003 and 2006–2014 were characterised by comparatively low activity. The peaks in 1997/98 and 2016 coincide with strong El Niño events in the Pacific Ocean (Figure 22). The Northern Hemisphere ACE values (central panel in Figure 45) dominate the global signal (lower panel) and therefore the peaks and lows are similar to the global data, without any clear

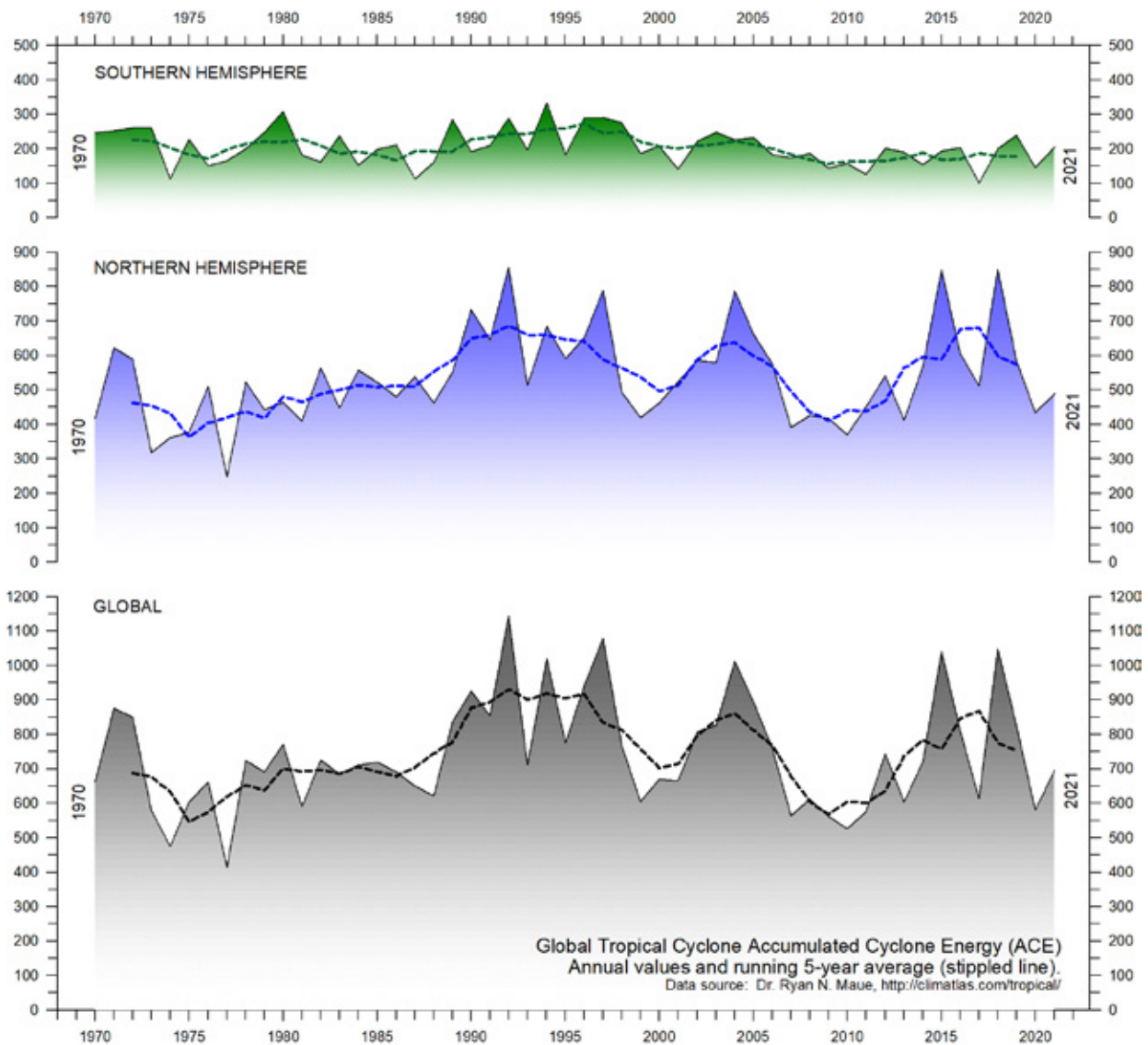


Figure 45: Annual global accumulated cyclone energy

Source: Ryan Maue.

trend over the length of the record. The Northern Hemisphere’s main cyclone season is June–November. The Southern Hemisphere ACE values (upper panel in Figure 45) are generally lower than for the Northern Hemisphere, and the main cyclone season is December–April.

The Atlantic Oceanographic and Meteorological Laboratory ACE data series goes back to 1850. A Fourier analysis (not shown here) for the Atlantic Basin (Figure 46) shows the ACE series to be influenced by periodic variations of about

55.8- and 7.8-years’ duration. The Atlantic Basin hurricane season often shows above-average activity when La Niña conditions are present in Pacific during late summer (August–October), as was the case in 2017 (Johnstone and Curry, 2017). The Eastern Pacific Basin data series is much shorter, starting in 1971, and is influenced by periods of 27.0- and 2.4-years’ duration. An ACE peak was apparently reached during 2015–18.

Other storm and wind observations

The number of hurricane landfalls in the continental United States is shown in Figure 47. The series shows considerable variations from year to year, but it is not possible to detect any clear trend over time. A Fourier analysis (not shown here) reveals a statistically significant period of about 3.2 years.

An insight into changes in prevailing wind conditions may be obtained from the inspection of observations carried out at coastal meteorological stations situated at particularly wind-exposed places. One example is Lista Lighthouse, in southernmost Norway. It sits on an exposed cape at the extreme southwestern edge of the mainland of Norway, well suited to register wind conditions in the adjoining North Sea and the European sector of the North Atlantic. It has a monthly wind record going back to January

1931, as displayed in Figure 48. This shows that peak wind strengths were recorded shortly after World War II and have since declined somewhat, to some degree mirroring the record of US hurricane landfalls (Figure 47); that is, on the opposite shore of the North Atlantic.

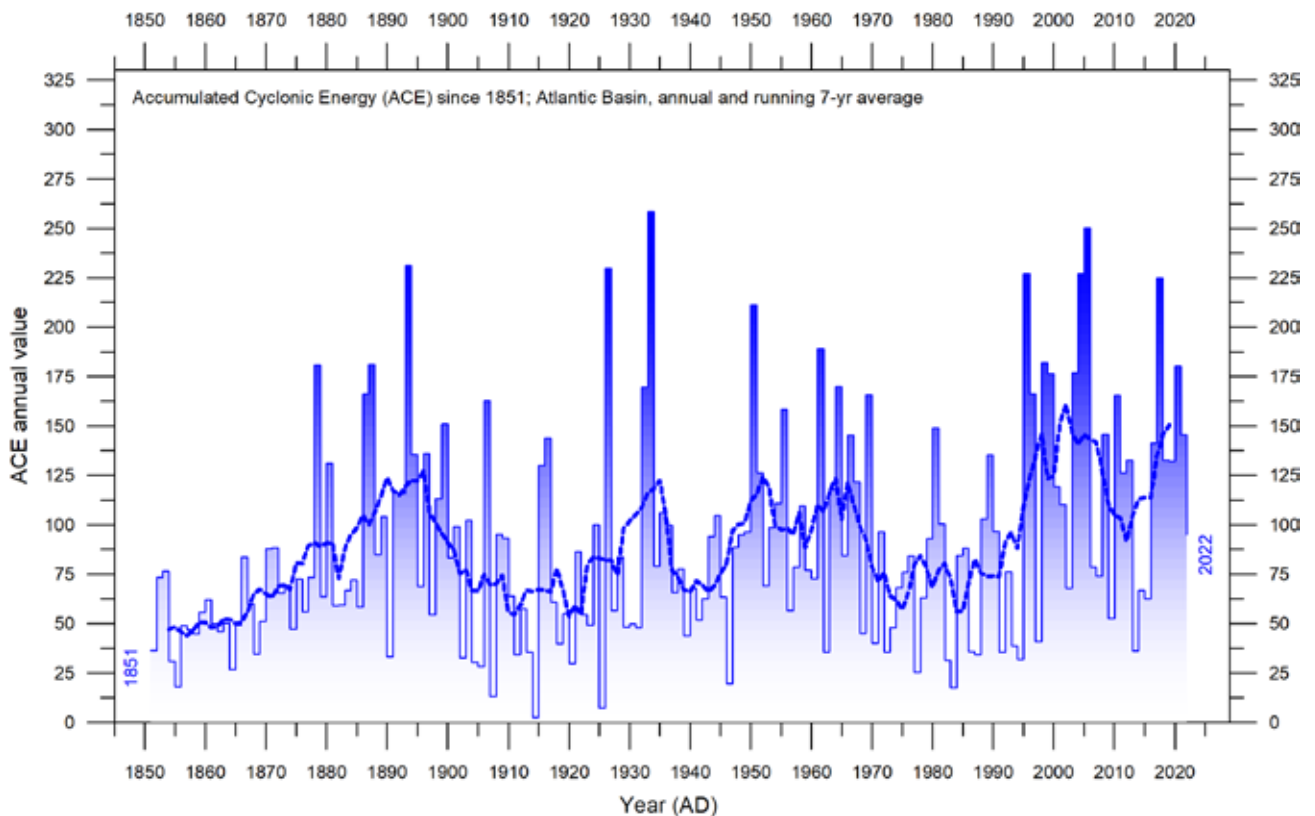


Figure 46: Atlantic Basin ACE since 1851

Thin lines show annual ACE values, and the thick line shows the running 7-year average. Data source: Atlantic Oceanographic and Meteorological Laboratory (AOML), Hurricane Research Division. Please note that these data are not yet updated beyond 2020.

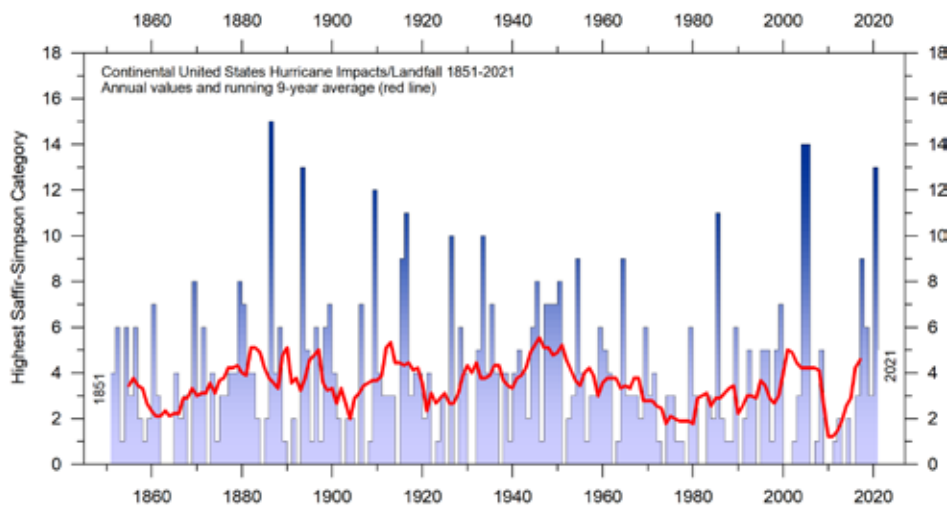


Figure 47: Hurricane landfalls in the continental United States 1851–2018

The highest Saffir-Simpson Hurricane Scale impact in the United States is based upon estimated maximum sustained surface winds produced at the coast. Data source: Hurricane Research Division, NOAA. Please note that this data series is not yet updated beyond 2018.

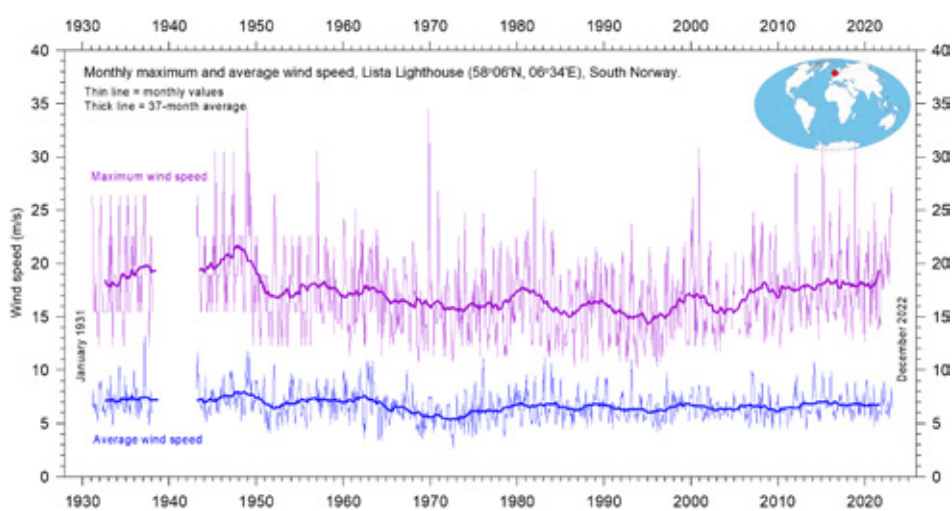


Figure 48: Monthly maximum and average wind speed since January 1931 measured at Lista Lighthouse, South Norway

Lista Lighthouse is situated on an exposed cape located at the extreme southwestern edge of mainland Norway, in a position to register wind conditions in the adjoining North Sea and the European sector of the North Atlantic. Data source: SeKlima.

Written references

- Carter R.M., de Lange W., Hansen, J.M., Humlum O., Idso C., Kear, D., Legates, D., Mörner, N.A., Ollier C., Singer F. and Soon W. 2014. *Commentary and Analysis on the Whitehead & Associates 2014 NSW Sea-Level Report*. Policy Brief, NIPCC, 24. September 2014, 44 pp. <http://climatechangereconsidered.org/wp-content/uploads/2014/09/NIPCC-Report-on-NSW-Coastal-SL-9z-corrected.pdf>.
- Chylek, P., Folland, C. K., Lesins, G., and Dubey, M. K. 2010. Twentieth century bipolar seesaw of the Arctic and Antarctic surface air temperatures. *Geophysical Research Letters*, 37: L08703, doi:10.1029/2010GL042793.
- Holgate, S.J. 2007. On the decadal rates of sea level change during the twentieth century. *Geophysical Research Letters*, 34: L01602, doi:10.1029/2006GL028492.
- Johnstone, J. and Curry, J. 2017. Causes and Predictability of the Exceptionally Active 2017 Atlantic Hurricane Season. Climate Forecast Applications Network (CFAN). https://curryja.files.wordpress.com/2017/11/hurricane_review_2017-final.pdf.
- Maue, R.L. 2011. Recent historically low global tropical cyclone activity. *Geophysical Research Letters*, 38, L14803, doi:10.1029/2011GL047711.
- Roemmich, D. and J. Gilson, 2009. The 2004–2008 mean and annual cycle of temperature, salinity, and steric height in the global ocean from the Argo Program. *Progress in Oceanography*, 82: 81–100.
- Turner et.al. 2017. Unprecedented springtime retreat of Antarctic sea ice in 2016. *Geophysical Research Letters*, 44(13): 6868–6875. <https://doi.org/10.1002/2017GL073656>.
- Vignudelli et al. 2019. Satellite Altimetry Measurements of Sea Level in the Coastal Zone. *Surveys in Geophysics*, 40: 1319–1349. <https://link.springer.com/article/10.1007/s10712-019-09569-1>.

Data sources

All sources were accessed January-February 2023.

ACE data: https://en.wikipedia.org/wiki/Accumulated_cyclone_energy.

AMO, Earth System Research Laboratory, NOAA, USA: <https://www.esrl.noaa.gov/psd/data/timeseries/AMO/>.

Atlantic Oceanographic and Meteorological Laboratory, Hurricane Research Division: <http://www.aoml.noaa.gov/hrd/tcfaq/E11.html>.

Continental United States Hurricane Impacts/Landfalls: https://www.aoml.noaa.gov/hrd/hurdat/All_U.S._Hurricanes.html.

Colorado Center for Astro dynamics Research: <http://sealevel.colorado.edu/>.

Danish Meteorological Institute (DMI): <http://ocean.dmi.dk/arctic/icethickness/thk.uk.php>.

Earth System Research Laboratory (ESRL): <https://www.esrl.noaa.gov/psd/map/clim/olr.shtml>.

SeKlima: <https://seklima.met.no/observations/>.

GISS temperature data: <https://data.giss.nasa.gov/gistemp/>.

Global Marine Argo Atlas: http://www.argo.ucsd.edu/Marine_Atlas.html.

Goddard Institute for Space Studies (GISS): <https://www.giss.nasa.gov/>.

HadCRUT temperature data: <http://hadobs.metoffice.com/>.

Hurricane Research Division, NOAA: <http://www.aoml.noaa.gov/hrd/tcfaq/E23.html>.

Hurricane Research Division, Continental United States Hurricane Impacts/Landfalls: https://www.aoml.noaa.gov/hrd/hurdat/All_U.S._Hurricanes.html.

National Ice Center (NIC): http://www.natice.noaa.gov/pub/ims/ims_gif/DATA/cursnow.gif.

National Snow and Ice Data Center (NSIDC): http://nsidc.org/data/seaice_index/index.html.

NCDC temperature data: <https://www.ncdc.noaa.gov/monitoring-references/faq/>.

Ocean temperatures from Argo floats: <http://www.argo.ucsd.edu/>.

Oceanic Niño Index (ONI): http://www.cpc.ncep.noaa.gov/products/analysis_monitoring/ensos-tuff/ensoyears.shtml.

Outgoing long wave radiation (OLR): <https://www.esrl.noaa.gov/psd/map/clim/olr.shtml>.

PDO, NOAA Physical Sciences Laboratory: <https://psl.noaa.gov/pdo/>.

Permanent Service for Mean Sea Level: <http://www.psmsl.org/>.

Phys.org 2019: <https://phys.org/news/2019-01-antarctica-sea-ice-climate.html>.

Plymouth State Weather Center: <http://vortex.plymouth.edu/sfc/sst/>.

PSMSL Data Explorer: <http://www.psmsl.org/data/obtaining/map.html>.

Rutgers University Global Snow Laboratory: <http://climate.rutgers.edu/snowcover/index.php>.

RSS temperature data: <http://www.remss.com/measurements/upper-air-temperature>.

Sea level from satellites: <https://sealevel.colorado.edu/data/2020rel1-global-mean-sea-level-seasonal-signals-retained>.

Sea level from tide-gauges: <http://www.psmsl.org/data/obtaining/map.html>.

Sea level modelled: IPCC AR6 Sea Level Projection Tool: https://sealevel.nasa.gov/data_tools/17.

Sea ice extent Danish Meteorological Institute (DMI): <http://ocean.dmi.dk/arctic/icethickness/thk.uk.php>.

Southern Oscillation Index (SOI): <http://crudata.uea.ac.uk/cru/data/soi/>.

Maue ACE data: climatlas.com/tropical/.

UAH temperature data: http://www.nsstc.uah.edu/data/msu/v6.0/tlt/uahncdc_lt_6.0.txt.

Review process

GWPF publishes papers in a number of different formats, with a different review process pertaining to each.

- Our flagship long-form GWPF Reports are all reviewed by our Academic Advisory Council.
- GWPF Briefings and Notes are shorter documents and are reviewed internally and/or externally as required.

Part of the function of the review process is to ensure that any materials published by the GWPF are of a proper academic standard, and will serve the GWPF's educational purpose. As a charity, we recognise that educational material should provide any reader the opportunity to understand, and explore different perspectives on a subject.

This means that, for most publications, we also invite an external review from a party who we would expect to take a different view to the publication's author. We offer to publish any substantive comments alongside the main paper, provided we are satisfied they will enhance the educational experience of the reader. In this way, we hope to encourage open and active debate on the important areas in which we work.

This enhanced review process for GWPF papers is intended to take the content and analysis beyond a typical review for an academic journal:

- More potential reviewers can be involved
- The number of substantive comments will typically exceed journal peer review, and
- The identity of the author is known to the potential reviewers.

As an organisation whose publications are sometimes the subject of assertive or careless criticism, this review process is intended to enhance the educational experience for all readers, allowing points to be made and considered in context and observing the standards required for an informed and informative debate. We therefore expect all parties involved to treat the reviews with the utmost seriousness.

Final responsibility for publication rests with the Chairman of the Trustees and the GWPF Director. But in every case, the views expressed are those of the author. GWPF has never had any corporate position beyond that dictated by its educational objectives.

About the Global Warming Policy Foundation

People are naturally concerned about the environment, and want to see policies that protect it, while enhancing human wellbeing; policies that don't hurt, but help.

The Global Warming Policy Foundation (GWPF) is committed to the search for practical policies. Our aim is to raise standards in learning and understanding through rigorous research and analysis, to help inform a balanced debate amongst the interested public and decision-makers. We aim to create an educational platform on which common ground can be established, helping to overcome polarisation and partisanship. We aim to promote a culture of debate, respect, and a hunger for knowledge.

THE GLOBAL WARMING POLICY FOUNDATION

Director

Benny Peiser

Honorary President

Lord Lawson

BOARD OF TRUSTEES

Dr Jerome Booth (Chairman)

The Hon. Tony Abbott

Lord Frost

Kathy Gyngell

Professor Michael Kelly FRS

Terence Mordaunt

Graham Stringer MP

Professor Fritz Vahrenholt

ACADEMIC ADVISORY COUNCIL

Professor Christopher Essex (Chairman)

Professor Wade Allison

Professor Anthony Barrett

Professor J. Ray Bates

Sir Ian Byatt

Dr John Constable

Professor Vincent Courtillot

Professor John Dewey

Professor Peter Dobson

Professor Peter Edwards FRS

Professor Samuel Furfari

Christian Gerondeau

Professor Larry Gould

Professor William Happer

Professor Ole Humlum

Professor Gautam Kalghatgi

Professor Terence Kealey

Bill Kininmonth

Brian Leyland

Professor Richard Lindzen

Professor Ross McKittrick

Professor Robert Mendelsohn

Professor Garth Paltridge

Professor Ian Plimer

Professor Gwythian Prins

Professor Paul Reiter

Professor Peter Ridd

Dr Matt Ridley

Sir Alan Rudge

Professor Nir Shaviv

Professor Henrik Svensmark

Dr David Whitehouse

RECENT GWPF REPORTS

20	Laframboise	Peer Review: Why Scepticism is Essential
21	Constable	Energy Intensive Users: Climate Policy Casualties
22	Lilley	£300 Billion: The Cost of the Climate Change Act
23	Humlum	The State of the Climate in 2016
24	Curry et al.	Assumptions, Policy Implications and the Scientific Method
25	Hughes	The Bottomless Pit: The Economics of CCS
26	Tsonis	The Little Boy: El Niño and Natural Climate Change
27	Darwall	The Anti-development Bank
28	Booker	Global Warming: A Case Study in Groupthink
29	Crockford	The State of the Polar Bear Report 2017
30	Humlum	State of the Climate 2017
31	Darwall	The Climate Change Act at Ten
32	Crockford	The State of the Polar Bear Report 2018
33	Svensmark	Force Majeure: The Sun's Role in Climate Change
34	Humlum	State of the Climate 2018
35	Peiser (ed)	The Impact of Wind Energy on Wildlife and the Environment
36	Montford	Green Killing Machines
37	Livermore	Burnt Offering: The Biomess of Biomass
38	Kelly	Decarbonising Housing: The Net Zero Fantasy
39	Crockford	The State of the Polar Bear Report 2019
40	Darwall	The Climate Noose: Business, Net Zero and the IPCC's Anticapitalism
41	Goklany	The Lancet Countdown on Climate Change: The Need for Context
42	Humlum	The State of the Climate 2019
43	Alexander	Weather Extremes: Are They Caused by Global Warming?
44	Constable	Hydrogen: The Once and Future Fuel?
45	Kessides	The Decline and Fall of Eskom: A South African Tragedy
46	Goklany	Impacts of Climate Change: Perception and Reality
47	Constable	A Little Nudge with a Big Stick
48	Crockford	The State of the Polar Bear Report 2020
49	Alexander	Weather Extremes in 2020
50	Humlum	The State of the Climate 2020
51	Humlum	The State of the Climate 2021
52	Constable	Europe's Green Experiment
53	Montford	Adaptation: The Rational Climate Policy
54	Alexander	Extreme Weather: The IPCC's Changing Tune
55	Ridd	Coral in a Warming World: Causes for Optimism
56	Humlum	The State of the Climate 2022

For further information about the Global Warming Policy Foundation, please visit our website at www.thegwpf.org.
The GWPF is a registered charity, number 1131448.

